Perovskite-Structure $TlBO_3$(B = Cr, Mn) for optoelectronic and thermo-mechanical application: A DFT investigation.

by

Wakil Hasan

Adeeb Mahamud Hossain

BACHELOR OF SCIENCE IN ELECTRICAL AND ELECTRONIC ENGINEERING

Department of Electrical and Electronic Engineering
INTERNATIONAL ISLAMIC UNIVERSITY CHITTAGONG

JULY 2022

Perovskite-Structure $TlBO_3$(B = Cr, Mn) for optoelectronic and thermo-mechanical application: A DFT investigation.

by

Wakil Hasan

Adeeb Mahamud Hossain

A thesis/project
submitted as partial fulfilment of the requirement for the degree of

BACHELOR OF SCIENCE IN ELECTRICAL AND ELECTRONIC ENGINEERING

Department of Electrical and Electronic Engineering
INTERNATIONAL ISLAMIC UNIVERSITY CHITTAGONG

JULY 2022

CERTIFICATE OF APPROVAL

The thesis/project entitled as "**Perovskite-Structure $TlBO_3$(B = Cr, Mn) for optoelectronic and thermo-mechanical application: A DFT investigation.**" submitted by **Wakil Hasan**, bearing Matric ID. **ET181037** and **Adeeb Mahamud Hossain**, bearing Matric ID. **ET181088** of session **Autumn 2021**, to the Department of Electrical and Electronic Engineering, International Islamic University Chittagong, has been accepted as satisfactory in partial fulfilment of the requirements for the degree of Bachelor of Science in Engineering and approved for the examination held on **22 July, 2022**.

_____

Supervisor
Md. Rasheduzzaman
Lecturer,
Department of Electrical and Electronic Engineering
International Islamic University Chittagong.

DECLARATION

It is hereby declared that this work has been done by us and no portion of the work contained in this thesis/project has been submitted elsewhere for the award of any degree or diploma.

_____

Wakil Hasan

_____

Adeeb Mahamud Hossain

ACKNOWLEDGMENT

All praises and thanks to Allah, the Lord of the world, the most Beneficent, the most Merciful for helping us to accomplish this work.

We are beholden to a number of people, who supported us to carry out this work regarding the outcome of this work (Thesis), we express our deepest sense of gratitude from the core of our heart to our honourable supervisor Md. Rasheduzzaman, Lecturer, Department of Electrical and Electronic Engineering, International Islamic University Chittagong for his scholastic supervision, valuable and scholastic guidance, constant encouragement profound cordiality and helpful discussion throughout the progress of this work. We hope we tried our best to reach our goal and this research work will help in future research on this field. We are highly grateful to him for allowing us to pursue this project under his supervision. We are grateful to the honourable chairman Dr. Sikder Sunbeam, and all teachers of the department of EEE for their constant support and encouragement. We are also thankful to all the staff of the department of EEE for their co-operation during preparing this paper. We express our heartiest thanks, especially to our all our seniors and all of our friends for their cooperation. Last but not least, we would like to thank those authors who we have mentioned and those who we haven't mentioned for their informative papers and materials. Finally, we are very much grateful to our parents and family members and well-wishers for their encouragement and support, which led us to complete this study.

Authors

ABSTRACT

First-principles-based DFT calculations have been carried out to analyse the structural, mechanical, elastic anisotropic, Vickers hardness, electronic, optical, and thermodynamic properties of $TlBO_3$(B = Cr, Mn) for the first time. We determined the lattice parameters, which are well accustomed to the previous results. The Born criteria are ensured by the elastic constants, also confirming ductility in the solid's nature. The elastic constants are also used to evaluate and analyse some related physical properties. The values of Vickers hardness are calculated to determine the hardness and relative application for both $TlCrO_3$ and $TlMnO_3$. Metallic characteristics are evaluated via the investigation of electronic band structure and density of states. Significant constants such as absorption, conductivity, reflectivity, dielectric, loss function, and refractive index are also considered and deliberated in specifics. As a result, various possible electronic, optical, and optoelectronic applications were predicted. $TlBO_3$(B = Cr, Mn) was also found to be reliable for thermal barrier coating (TBC) as the evaluated value of thermal conductivity and Debye temperature indicates.

TABLE OF CONTENTS

LIST OF FIGURES

LIST OF TABLES

LIST OF ABBREVIATIONS

Ab initio	From the beginning (Latin Term "*ab initio*")
BZ	Brillouin Zone
CASTEP	CAmbridge Serial Total Energy Package
DFT	Density Functional Theory
DOS	Density of States
eV	Electron Volts
Fig.	Figure
Expt.	Experimental Data
GGA	Generalized Gradient Approximation
LDA	Local Density Approximation
GPa	Giga Pascal
PBE	Perdew-Burke-Ernzerhof
PDOS	Partial Density of States
TDOS	Total Density of States
MIT	Metal-insulator-transition
CMR	Colossal magnetoresistance
GMR	Giant magnetoresistance
TBC	Thermal Barrier Coating

CHAPTER 1

INTRODUCTION

1.1 Introduction

A perovskite is a solid material that consists the crystal structure ABX_3. It was first revealed as the mineral called perovskite, that was $CaTiO_3$ [1]. This mineral was discovered in the Ural Mountains located in Russia by Gustav Rose in 1839 and named after Russian mineralogist L. A. Perovski. A and B in the crystal structure are two ions of different sizes, and X is an ion that bonds to both ions. The A atoms are usually larger than the B atoms. The cubic structure has the B cation in 6-fold coordination, as a result surrounded by an octahedron of anions, and the A cation in 12-fold cuboctahedra coordination. In addition, perovskite forms may exist where either/both the A and B sites have a configuration of $A1_{x-1}A2_x$ and/or $B1_{y-1}B2_y$ and the X is most of the time is Oxygen as it bonds with both A and B ions properly [2].

Physical properties of attention to solid materials science among perovskites embrace superconductivity, magnetoresistance, ionic conductivity, and a multitude of dielectric properties. These dielectric properties are of great significance in microelectronics and telecommunication. They are also some interests for scintillator as they have large light yield for radiation conversion. Because of the flexibility of bond angles inherent in the perovskite structure there are many different types of alterations which can occur from the ideal structure. These include tilting of the octahedra, displacements of the cations out of the centres of their coordination polyhedral, and alterations of the octahedra driven by electronic factors called Jahn-Teller distortions [3].

Perovskite structures are accepted by oxides that have the chemical formula ABO_3. The idealized form is a cubic structure (space group Pm3m, no. 221) which is rarely encountered. The orthorhombic (e.g., space group Pnma, no. 62, or Amm2, no. 68) and tetragonal (e.g., space group I4/mcm, no. 140, or P4mm, no. 99) phases are the most common non-cubic variants. The perovskite structure is named after $CaTiO_3$, these mineral forms a non-idealized form. $SrTiO_3$ and $CaRbF_3$ are examples of cubic perovskites. Barium titanate is an example of a perovskite which can take on the rhombohedral (space group R3m, no. 160), orthorhombic, tetragonal and cubic forms depending on temperature [4]. General categories of cation-pairing possible can be classified as four types: $A^{+}B^{2+}X^{-}{}_3$, 1:2 perovskites; [5] $A^{2+}B^{4+}X^{2-}{}_3$, 2:4 perovskites; $A^{3+}B^{3+}X^{2-}{}_3$, 3:3 perovskites; and $A^{+}B^{5+}X^{2-}{}_3$, or 1:5 perovskites. The relative ion size

necessities for stability of the cubic structure are quite stringent. Off-cantering of an undersized B cation within its octahedron allows it to attain a stable bonding pattern. The resulting electric dipole is responsible for the property of ferroelectricity and shown by perovskites such as $BaTiO_3$ that distort in this fashion.

1.2 Target of the Present Study

The target of the present study is to examine the structural, elastic, anisotropic electronic, Vickers hardness, optical, and thermodynamic properties of $TlBO_3$(B = Cr, Mn). The main purpose of the study is to determine the equilibrium structure. From which the equilibrium volume, bulk modulus, elastic constant, band structures, total and partial density of state (DOS), optical properties, will be calculated. Then compare the calculated values of Both orthorhombic $TlCrO_3$ and triclinic $TlMnO_3$ with other theoretical and experimental values that are available.

1.3 Outline of the Project

The project is outlined as follows:

1 The general introduction of the present work is given in chapter one.

2 The chapter two deals with the Literature Review of Perovskite materials and $TlBO_3$(B = Cr, Mn).

3 The Crystal structure for both orthorhombic $TlCrO_3$ and triclinic $TlMnO_3$ are presented in chapter three

4 The methods of calculation which are used to study both $TlCrO_3$ and $TlMnO_3$ are described in chapter four.

5 The computation of different properties of $TlBO_3$(B = Cr, Mn) is given in chapter five.

6 The results of various investigations of the study are mentioned and displayed in chapter Six.

7 The conclusions of the thesis are given in chapter seven.

CHAPTER-2

LITERATURE RIVIEW

2.1 Introduction

The purpose of a literature review is to gain an understanding of the existing research and debates relevant to a particular topic or area of study, and to present that knowledge in the form of a written report which we have done in this chapter. Conducting a literature review helped us build our knowledge in this field.

2.2 Literature review

Perovskite oxides (ABO_3) are a point of interest for scientific researchers for their phase transformation and significant applications in modern technology [6]–[10]. ABO_3 structure type perovskites were extensively explored for metal-insulator transitions(MITs) correlating transition metal oxides [11]–[19]. $La_{1-x}B_xMnO_3$(B = Mn, Ca) perovskite magnates are well known to show the MITs with ferromagnetic-paramagnetic transition [20]. Perovskite materials are also found to be suitable for solid oxide fuel cells [21], [22]. ABO_3 is considered ideal perovskite material where A is a monovalent otherwise divalent cation situated on the edges of the crystal, and B is a tetravalent or pentavalent transition metal [23], [24]. Kim *et al.* discussed the structural distortion of ABO_3 type perovskite owing to a disparity among the A-O and B-O bond distances [25]. A cation on structural distortion and physical properties is hard to investigate as Kim *et al.* agreed because rare earth and yttrium ions bond to oxygen with parallel covalency. As a result, Tl (III), a post-transition metal ion is a decent choice for A cation in ABO_3 perovskites for its full occupation of 4*f* and 5*d* orbits ([XE] = $4f^{14}\ 5d^{10}\ 6s^2\ 6p^1$) in distinction to rare-earth ions ([XE] = $4f^{\,n}\ 5d^0\ 6s^0$; $0 \leq n \leq 14$). The transition metals in the B site of ABO_3 perovskite make the material suitable for any application such as high-temperature superconductivity, colossal magnetoresistance(CMR), charge ordering, giant magnetoresistance(GMR), piezoelectricity, ferroelectricity and so on [26]–[29]. ABO_3 perovskite oxides are also a great point of interest because of their use in constructing infrared sensors, optoelectronic modulators, infrared detectors, microwave devices, and different electro-mechanical systems [30]–[33]. Tl(III) compounds such as $TlFeO_3$ and $TlCrO_3$ were formulated five decades back[34] but further investigation lacks due to the difficulty of preparation. So, it is exciting to further study $TlBO_3$(B = Cr, Mn) structure type perovskites.

$ACrO_3$(A = Sc, I, Tl, Bi) [35]–[39] perovskite-type chromite which is significantly different in properties from isostructural chromite $RCrO_3$(R = rare earth elements). It can result from the distortion of the crystal structure ($ScCrO_3$, $InCrO_3$), chemical bonds ($TlCrO_3$, $BiCrO_3$) in these compounds, and the electronic structure of A^{3+} [40]. $RCrO_3$ compounds were found to exhibit spin reorientation transition, good oxygen-ion conduction (doped), and sensitivity towards methanol, ethanol, some gases, and humidity [41]. $R^{3+}Mn^{3+}O_3$ were investigated for their multiferroic properties in both perovskites and hexagonal modification [42]–[47] and rich magnetic phases [46]. $RCrO_3$(R = Gd, Tb, Er, Tm, Sn, and Y) [48], [49] showed large polarization at a high temperature equivalent to the Neel temperature (T_N) of the Cr subsystem, and $LaCrO_3$, $CeCrO_3$ displayed high T_N in $RCrO_3$ structure type materials [50]. Orthorhombic $RMnO_3$(R = Tb, Dy) [42], [51] which are spiral magnets that displayed magnetoelectric(ME) coupling. $DyFeO_3$ was investigated by Tokunaga *et al* and found to be versatile with gigantic ME phenomena [52].

Paul *et al.* analysed ABO_3 perovskites like $BiNiO_3$ or $PbCrO_3$ [53] for MITs and different investigations of A, and B ions led to the proposition of two more candidates in this category namely, $TlMnO_3$ and $InMnO_3$. Yi *et al.* investigated and synthesized $TlCrO_3$ [36] and $TlMnO_3$ [54] with Mössbauer spectroscopy with high pressure (6GPa) and high temperature (1500K) and found separate structural and magnetic properties where the absence of spin canting suggested $TlCrO_3$ have non-trivial magnetic structure. Khalyavin *et al.* also studied the magnetic structure of $TlMnO_3$ [55] under the same amount of high temperature and pressure by applying the neutron diffraction technique and confirmed anisotropic exchange interactions that revealed the Jahn Teller distortion playing a key role in creating the magneto-crystalline anisotropy. Belik investigated manganese-oxide-based $Bi_{1-x}Y_xMnO_3$ with high pressure and high temperature [56]. R_2O_3-In_2O_3 systems were studied at normal pressure and some ABO_3 compounds were found that contained I^{3+} or Tl^{3+} [57], [58]. On that criteria, Shannon synthesized some perovskite containing In and Tl that includes $InCrO_3$, $TlCrO_3$, and $TlFeO_3$ [34]. Ab initio study was performed on many perovskites including $BaMO_3$(M = Pr, Th, U) [59], $SnTaO_3$ [26], ACO_3(A = Ca, Sr) [60], and $SrHfO_3$ [61] Z. Hasan *et al.* investigated ABO_3 structure type perovskite $AMoO_3$ [62] where A is Ca, Sr, $SrBO_3$ [63] where B is Cr, Fe and $SrFeO_3$ [64] with density functional theory (DFT) and found it mechanically stable under different pressure along with other physical properties. $LnCrO_3$ [65]–[67] which crystallizes in $GdFeO_3$ and

$BiFeO_3$ with similar structure type perovskites were studied and found to have application in thin-film devices. $LaNiO_3$ reveals metallic nature along with Pauli para-magnetism. $LuNiO_3$ and $YNiO_3$ on the other hand display Curie-Weiss para-magnetism with antiferromagnetic order which is below T_N [68]. $TlNiO_3$ perovskite was synthesized under high pressure and a relative study was performed with $TNiO_3$(T = rare earth) [69]. According to Cao *et al.,* chromium oxide-based $CeCrO_3$ [70] which is rare earth orthochromite shows magnetic properties and anti-ferromagnetism. $LaCoO_3$ with ABO_3 structure type was studied for a lengthy period for its spin-state transition and electronic or ionic conductivity [71]. Mn^{3+} based perovskite $TlMnO_3$ has been described to have a triclinic crystal structure with a clear signature of Jahn-Teller distortion [54]. Ding *et al.* investigated $TlCrO_3$, $InCrO_3$, and $ScCrO_3$ with high pressure and high-temperature settings which revealed the orthorhombic structure of these materials [72].

In this experiment further investigation of ABO_3 structure-based $TlBO_3$(B = Cr, Mn) is done where Tl is a post-transition metal, Cr and Mn are transition metals and O is a non-metal. ABO_3 structure-based perovskite shows unique physical properties that use various types in modern technology, motivating us to properly analyse uncovered physical properties. This paper studies the physical properties like structural, mechanical, elastic anisotropic, electronic, thermal, Vickers hardness, and optical properties of $TlCrO_3$ and $TlMnO_3$, based on the analysis of Band structure, Density of states, elastic constants, and dielectric functions by DFT base CAmbridge Serial Total Energy Package (CASTEP). The main focal purpose of this investigation is to analyse the mentioned physical properties of the perovskites that can be subjugated to different usages.

2.3 Contribution

First-principal based DFT calculation have been done for the first time for both $TlCrO_3$ and $TlMnO_3$. The structural investigation is in good amenability with previous results. Physical properties such as elastic anisotropy, electronic properties, Vickers's hardness, optical properties, and thermodynamic properties are calculated for the first time and many applications are predicted.

CHAPTER-3

CRYSTAL STRUCTURE OF $TlBO_3$(B = Cr, Mn)

3.1 Introduction

The spacing of atoms in the material performs a key role in deciding many properties such as electronic band structure and optical properties of the materials. Materials can be branched into two sections by the way of the arrangement of atoms in a material. An amorphous solid has no definite form, either geometric or crystalline. An amorphous solid is any non-crystalline solid that does not organize the atoms and molecules in a definite lattice pattern. Another group is called polycrystalline materials. Polycrystalline materials are solid that consist of many small crystals (the grain). The grains are separated by grain boundaries and normally have random crystals that can be described in terms of a lattice, with a group of atoms attached to every lattice point. Crystals can be divided by their crystal structure and underlying lattice. One single atom is enough to consist of one lattice point. Each lattice point may consist of one single atom (copper, silver, etc.), however with most materials, it consists of a combination of atoms or molecules. The structure of all crystals can be described in terms of a lattice, with a group of atoms attached to every lattice point. The group of atoms is called the basis; when repeated in space it forms the crystal structure.

Crystal structure = Lattice + Basis

The basis consists of a primitive cell, containing one single lattice point. Arranging one cell at each lattice point will fill up the entire crystal. The unit cell is given by its lattice parameters, the length of the cell edges, and the angles between them, while the positions of the atoms inside the unit cell are described by the set of atomic positions (x_i, y_i, z_i) measured from a lattice point.

We have designated the crystal structure of $TlCrO_3$ and $TlMnO_3$ in this chapter. The objective of this chapter is to give a clear conception of the crystal structure of the compound under investigation.

3.2 Crystal Structure

$TlBO_3$(B=Cr, Mn) perovskite materials prepared with stoichiometric mixtures of Cr_2O_3(for $TlCrO_3$), Fe_2O_3(for $TlMnO_3$) and Tl_2O_3 [36], [54]. Both materials share the same $TlBO_3$ ionic structure but both share different crystal structure types. **Figure3.1** illustrates the Crystal structure of $TlBO_3$(B = Cr, Mn). $TlCrO_3$ crystalizes in orthorhombic structure by means of space group Pnma (no. 62). In $TlCrO_3$ for Tl site 4*c*

Wyckoff position (0.04617, 0.25, 0.98732), Cr site 4b Wyckoff position (0, 0, 1/2) and for O there are two site, for the first one 4c Wyckoff position (0.4504, 0.25, 0.1050) and for the second 8d Wyckoff position (03009, 0.0558, 0.6969)[36]. $TlMnO_3$ crystalizes in triclinic structure with space group $P\bar{1}$(no. 2). In $TlMnO_3$, Tl site has 2*i* (0.54745, 0.25794, 0.50994) and 2*i* (0.04935, 0.24233, 0.97513). For Mn atoms are positioned in 4 sites. Mn1, Mn2, Mn3 and Mn4 has 1*d* (1, 0.5, 0, 0); 1e (1, 0.5, 0.5, 0); 1*b* (1, 0, 0, 0.5); 1*g* (1, 0, 0.5, 0.5) respectively. O atoms are positioned in 6 site O(1-6) which are in numerical order as follows, 2*i* (for all sites) Wyckoff position (0.9423, 0.2309, 0.3799); (0.4450, 0.2708, 0.1147); (0.2056, 0.5732, 0.2055); (0.8053, 0.0511, 0.8070); (0.2824, 0.4406, 0.6847); (0.6839, 0.9275, 0.2855) respectively [54]. The optimized lattice parameters a, b and c are presented in **Table 6.1** along with calculated unite cell volume V. The obtained results are associated with former results and seems to be in good amenability with those outcomes, which indicates our calculations to be reliable. Both materials share different crystals structures, but the calculated lattice constants are pretty close. The Volume for both $TlCrO_3$ and $TlMnO_3$ are calculated and seems to have near lattice constant values.

3.2.1 Lattice Parameters

The lattice parameter (or lattice constant) refers to the lattice constant distance between unit cells in a crystal lattice. Lattices in three dimensions generally have three lattice constants, referred to as *a*, *b*, and *c*. The angles *α*, *β*, and γ denote the angles between the vectors *b* and *c*, *c* and *a*, *a* and *b*, respectively. A group of lattice constants could be referred to as lattice parameters. However, the full set of lattice parameters consists of the three lattice constants and three angles between them. In $TlCrO_3$ and $TlMnO_3$ the lattice parameters $a \neq b \neq c$. The lattice parameters for Laves phases $TlBO_3$(B = Cr, Mn) are given in **Table 6.1**.

3.2.2 Structural Unit

Crystallography is a unit cell of minimum volume, A parallel pipe-shaped volume whose edges are defined by the primitive translation of a crystal lattice. A primary cell is built on the basis vectors L such that every lattice vector t of L may be obtained as an integral linear combination of the basis vectors a, b, and c. It contains only one lattice point and its volume is equal to the triple scalar product. We know that a unit cell is a structural arrangement of atoms, which is the surface in three-dimensional spaces to describe the

crystal. This indicates that a unit cell is a region of the crystal defined based on vectors a, b and c so that if this region is translated by an integral multiple of any vector, the region will be similar to the crystal. In this case, the unit cell is multiple cells and has multiple lattice points. The abundance of cells is given by the ratio of the volume of a primitive cell to its volume. A primitive cell is a type of cell or single cell that has a minimum volume. There are many ways to select a unit or primitive cell for a given crystal system. There are many ways of choosing a unit or primitive cell for a given crystal system. The number of atoms per unit cell must be the same for a particular crystal structure i.e., the number of atoms in a unit cell is independent of the process by which the unit cell is chosen. By repetition of the unit cell with suitable symmetry operations, the full structure of the crystal can be obtained. Thus, the unit cell can be defined as the fundamental structural unit of the crystal. To know the properties of a crystal, it is only sufficient to know the properties of a unit cell of the crystal.

In crystallography, the orthorhombic and triclinic crystal systems are two of the seven lattice point groups. The volume of both unit cell is $V=abc$ $Å^3$. The unit cell is marked in the crystal structure of $TlBO_3$(B = Cr, Mn) in **Figure 6.1**.

CHAPTER-4

METHODS OF CALCULATION

4.1 Introduction

At present research world, atomistic and electronic structure calculations have become more essential field than past decade, especially with high-performance computers and a race to improve every invention. It is sometimes more convenient to carry out computer calculations than analytical experiments. Among the many fields in condensed matter physics where this approach can be exploited, we have a special interest in the study of the pressure behaviour of very hard materials. Usually, extremely high pressures are needed for the study of such materials in order to induce some significant change in their structures. At static pressure, the production of hydrostatic conditions is not always possible and the samples are necessarily very small. If we want to know the atomic structure of the material, electronic properties and how can we modify the bonding between atoms or the material's chemical content to create new materials with properties of the component. A number of methods can be used. It can be divided into two classes: *ab initio* or first-principles methods, like density functional theory (DFT), and empirical or semi-empirical methods, like empirical tight-binding (ETB).

Ab initio or first principal methods use no experimental parameters in their computations. Instead, their computations are based solely on the laws of quantum mechanics and on the values of a small number of physical constants. Alternatively, Semi-empirical methods use parameters obtained from experimental data to simplify the calculations. They solve an approximate form of the Schrödinger equation that depends on having appropriate parameters available for the type of the system under investigation. Different semi-empirical methods are largely characterized by their different parameter sets.

The *ab initio* or first principal methods are useful in predicting the properties of new materials such as the evaluation of the energy levels of electrons in solids, which used to know the energy bands, which is the central theoretical problem of solid-state physics. The investigation of $TlBO_3$(B= Cr, Mn) is done with the most commonly used first-principle modelling of structural, electronic, and optical properties Density Functional Theory (DFT) with the periodic ambient condition along with generalized gradient approximation (GGA) and Perdew-Burke-Ernzerhof (PBE) exchange-correlation functional [73]–[75] using the Cambridge Serial Total Energy Package (CASTEP) code [76]. The atomic calculations for Tl – $6s^2 6p^1$, Cr – $3d^5 4s^1$, Mn – $3d^5 4s^2$ and O – $2s^2 2p^6$

are executed. The Brillouin zone *k*-points sampling is taken using the Monk-horst-Pack scheme [77] with 10 × 7 × 10 grid points for $TlCrO_3$ and 7 × 5 × 7 grid points for $TlMnO_3$. The plane-wave Cut-off energy is 450eV and 400eV for $TlCrO_3$ and $TlMnO_3$ respectively. The Broyden-Fletcher- Goldfarb-Shanno (BFGS) minimization method also known as the quasi-Newton method [78] is employed as a method of optimization of the crystal. The principles of convergence for the optimization are set to 1×10^{-5}eV per atom for total energy, 0.03 eV/Å for maximum force, and 0.05 GPa for maximum stress. The stress-strain method [79] is used to attain the elastic stiffness constants of $TlBO_3$(B= Cr, Mn) using CASTEP. The Yong's modulus, shear modulus along with Poisson's ratio presented in the 3D anisotropy models are obtained using the ELATE program [80]. Lastly, the electronics properties are evaluated by setting the above-mentioned parameters.

In this research, the calculations were accomplished utilizing an *ab initio* plane wave pseudopotential (PWPP) method in the framework of density functional theory (DFT) using generalized gradient approximation (GGA) (implemented in CASTEP code [81]) in order to investigate structural, electronic and optical properties. The rigorous mathematical procedures of the *ab initio* methods are discussed in details in the present chapter.

4.2 Wave Function

A wave function or wave function is probability amplitude in quantum mechanics describing the quantum state of a particle and how it behaves. Typically, its values are complex numbers and, for a single particle, it is a function of space and time. The laws of quantum mechanics (the Schrödinger equation) describe how the wave function evolves over time.

It is denoted by the most common symbol ψ (position, time) and where $|\psi|^2$ is equal to the chance of finding the subject at a certain time and position.

4.3 Atomic Orbital's and Bloch Function

The atomic orbital model is the currently accepted model of the electrons in an atom. It is sometimes called the wave mechanic's model. In the atomic orbital model, the atom consists of a nucleus surrounded by orbiting electrons. These electrons exist in atomic orbital, which are a set of quantum states of the negatively charged electrons trapped in the electrical field generated by the positively charged nucleus. However, the atomic

orbital model can only be described by quantum mechanics, in which case the electrons are more accurately described as standing waves surrounding the nucleus. An atomic orbital is a mathematical function that describes the wave-like behaviour of either one electron or a pair of electrons in an atom. This function can be used to calculate the probability of finding any electron of an atom in any specific region around the atom's nucleus [82]. These functions may serve as three-dimensional graphs of an electron's likely location. The term may thus refer directly to the physical region defined by the function where the electron is likely to be. Specifically, atomic orbitals are the possible quantum states of an individual electron in the collection of electrons around a single atom, as described by the orbital function [83].

The Bloch functions are summarized as follows:

» The Eigen vectors of the periodic Hamiltonian must satisfy the Bloch theorem.

» Different Eigen functions can satisfy the Bloch theorem for the same k-value; this implies that the Eigen-vectors of our Hamiltonian are also levelled with an *n* index.

» There are as many solutions as there are non-equivalent k-points: the number of k-points is N, the number of cells in the crystal. As the crystal size increases, the k-points get closer and closer; at the limit of infinite lattice, k becomes a continuous variable that can take all the possible values within Brillouin Zone (BZ).

4.4 The Schrödinger Equation

The Schrödinger equation is the fundamental equation of physics for describing quantum mechanical behaviour. It is also often called the Schrödinger wave equation, and is a partial differential equation that describes how the wave function of a physical system evolves over time. Viewing quantum mechanical systems as solutions to the Schrödinger equation is sometimes known as the Schrödinger picture, as distinguished from the matrix mechanical viewpoint, sometimes known as the Heisenberg picture.

Both density functional theory and wave function mechanics start with the formulation of the time-independent Schrödinger equation [84].

$$\hat{H}\Psi = E\Psi \tag{4.1}$$

where Ψ is the wave function, which contains all the information on the system described, $\hat{H}$ is the Hamiltonian operator which operates on the wave function and presents an output *E*, the total energy of the system, as its eigenvalue. There are several other operators available, for example for spin, electric dipole moments and so on. These can be used to obtain expectation values of physical observables from the wave function.

4.5 Plane Wave Basis Sets

Atomic orbitals are mathematical functions that describe the behaviour of the electron density of the different orbital's, 1*s*, 2*s*, 2*p* and so on, of an atom. They consist of functions, a basis set, that are combined to accurately represent the way electrons behave in space as well as ideally being reasonably quick to use in calculations.

In addition to localized basis sets, plane-wave basis sets can be used in quantum-chemical simulations. Typically, a finite number of plane-wave functions are used, below a specific cut-off energy which is chosen for a certain calculation. These basis sets are popular in calculations involving periodic boundary conditions. Certain integrals and operations are much easier to code and carry out with plane-wave basis functions than with their localized counterparts. In practice, plane-wave basis sets are often used in combination with an 'effective core potential' or pseudopotential, so that the plane waves are only used to describe the valence charge density. This is because core electrons tend to be concentrated very close to the atomic nuclei, resulting in large wave function and density gradients near the nuclei which are not easily described by a plane-wave basis set unless a very high energy cut-off, and therefore small wavelength, is used. This combined method of a plane-wave basis set with core pseudopotential is often abbreviated as a PSPW calculation. Furthermore, as all functions in the basis are mutually orthogonal, plane-wave basis sets do not exhibit basis-set superposition error. However, they are less well suited to gas-phase calculations. Using Fast Fourier Transforms, one can work with plane-wave basis sets in reciprocal space in which not only the aforementioned integrals, such as the kinetic energy, but also derivatives are computationally less demanding to be carried out. Another important advantage of a plane-wave basis is that it is guaranteed to converge to the target wave function while there is no such guarantee for Gaussian-type basis sets.

4.6 Linear Combinations of Atomic Orbital's

A linear combination of atomic orbital's or LCAO is a quantum superposition of atomic orbital's and a technique for calculating molecular orbital's in quantum chemistry [85]. In quantum mechanics, electron configurations of atoms are described as wave functions. In mathematical sense, these wave functions are the basis set of functions, the basic functions, which describe the electrons of a given atom. An initial assumption is that the number of molecular orbitals is equal to the number of atomic orbitals included in the linear expansion. In a sense, atomic orbitals combine to form in molecular orbital's, which can be numbered i = 1 to n and which may not all be the same. The expression (linear expansion) for the i the molecular orbital would be:

$$\Phi = \sum_{i=1}^{n} a_i \varphi_i \tag{4.2}$$

The coefficients, a_i, used to describe the contribution of each atomic orbital, φ_i, to the molecular orbital's, Φ, are what is solved for.

4.7 The Variational Principle

A variational principle is a scientific principle used within the calculus of variations, which develops general methods for finding functions which minimize or maximize the value of quantities that depends upon those functions. There exist an infinite number of solutions to the electronic Schrödinger equation, with the accurate solution being the one which minimizes the energy of the system, i.e., which gives the lowest energy solution to the equation. Working within the Born-Oppenheimer approximation the goal is to find the ground state energy of the system by finding the wave function that minimizes the energy of the entire system.

4.8 Pauli Principle

Spin is an inherent property of electrons, and each electron is characterized by a spin quantum number, ± ½, frequently called α and β. Spin can be introduced in many different ways into quantum theory, the most common being through the application of relativity, where the concept is introduced in a natural way as a result of the Dirac equations [86]. Relativity also introduced the Pauli principle, which states that no two electrons can have the same four quantum numbers; that is, if n, l, and m_l are the same, m_s must be different such that the electrons have opposite spins. More generally, no two identical fermions (particles with half-integer spin) may occupy the same quantum state simultaneously. A more rigorous statement

of this principle is that for two identical fermions, the total wave function is anti-symmetric. An anti-symmetric wave function is one in which the sign of the wave function changes when two electrons exchange coordinates. A useful tool in constructing wave functions with the correct anti-symmetric properties is Slater determinants.

4.9 Slater Determinant

In quantum mechanics, a Slater determinant is an expression which describes the wave function of a multi-fermionic system that satisfies anti-symmetry ($\Phi = 0$) requirements and subsequently the Pauli exclusion principle by changing sign upon exchange of fermions, the general form which is shown in equation (3.3). N is the number of electrons and χ is a spin-orbital, the product of a spatial orbital and a spin eigen function. This notation gives both a mathematically useful expression as well as a representation that is consistent with Pauli principle [87].

$$\Psi_{SD} = \frac{1}{\sqrt{N!}} \begin{vmatrix} \chi_1(1) & \cdots & \chi_N(1) \\ \vdots & \ddots & \vdots \\ \chi_1(N) & \cdots & \chi_N(N) \end{vmatrix} \tag{4.3}$$

4.10 Ab initio Method

Ab initio is a Latin term meaning "from the beginning" and is derived from the Latin word '*ab'* (from) and *'initio'*, ablative of initium (beginning). A method of calculating atomic and molecular structure directly from the first principles of quantum mechanics, without using quantities derived from experiment (such as ionization energies found by spectroscopy) as parameters. *Ab initio* calculations require a large amount of numerical computation; the amount of computing time required increases rapidly as the size of the atom or molecule increases. The development of computing power has enabled the properties of both small and large molecules to be calculated accurately, so that this form of calculation can now replace semi-empirical calculations. *Ab initio* calculations can, for example, be used to determine the bond lengths and bond angles of molecules by calculating the total energy of the molecule for a variety of molecular geometries and finding which conformation has the lowest energy.

The simplest type of *ab initio* electronic structure calculation is the Hartree–Fock (HF) scheme, in which the instantaneous Coulombic electron-electron repulsion is not specifically taken into account. Only its average effect (mean field) is included in the calculation. This is a variational procedure; therefore, the obtained approximate energies, expressed in terms of the system's wave function, are always equal to or greater than the

exact energy, and tend to a limiting value called the Hartree–Fock limit as the size of the basis is increased [88]. Many types of calculations begin with a Hartree–Fock calculation and subsequently correct for electron-electron repulsion, referred to also as electronic correlation. Møller–Plesset perturbation theory (MPn) and coupled cluster theory (CC) are examples of these post-Hartree–Fock methods [89]. In some cases, particularly for bond breaking processes, the Hartree–Fock method is inadequate and this single-determinant reference function is not a good basis for post-Hartree–Fock methods. It is then necessary to start with a wave function that includes more than one determinant such as multi-configurational self-consistent field (MCSCF) and methods have been developed that use these multi-determinant references for improvements [88].

With a given chemical composition and crystalline structure for any periodic system, the *ab initio* method is used to calculate the physical and chemical properties of the system as accurately as possible without any need for a priori information. In this method the fundamental approximation made is the expansion of the single particle wave functions (Crystalline orbital, CO) as a linear combination of Bloch functions (BF) defined in terms of local functions (Atomic orbital, AO). The local functions are, in turn, linear combinations of Gaussian type functions (GTF) whose exponents and coefficients are defined by input [90]. When approximations are sufficiently small in magnitude, *ab initio* methods have the advantage that they can be made to converge to the exact solution. The convergence, however, is not monotonic, and sometimes the smallest calculation gives the best result for some properties.

The most popular classes of *ab initio* methods are:

- Hartree-Fock (HF) method.
- Density Functional Theory (DFT).

4.10.1 Hartree-Fock (HF) method

The Hartree–Fock (HF) method is an approximate method for the determination of the ground-state wave function and ground-state energy of a quantum many-body system. First formulated in 1928 by Hartree [91] and then corrected to include the Pauli principle in 1930 by Fock and Slater, the method is the way in which many quantum chemical problems are solved, even though it is usually carried out in the matrix formulation proposed by Roothaan in 1951 [92]. The procedure consists of a few distinct steps; starting with the Slater determinant for an electronic configuration the Hartree-Fock equations are set up. The Fock operator and the secular equation is formulated and solved iteratively until self-consistency

is achieved. A ground state energy minimum should thus have been found. The Hartree–Fock method assumes that the exact, N-body wave function of the system can be approximated by a single Slater determinant (in the case where the particles are fermions) or by a single permanent (in the case of bosons) of N spin-orbitals. By invoking the variational principle, one can derive a set of N-coupled equations for the N spin orbitals. Solution of these equations yields the Hartree–Fock wave function and energy of the system, which are approximations of the exact ones.

The Hartree–Fock method finds its typical application in the solution of the electronic Schrödinger equation of atoms, molecules, and solids but it has also found widespread use in nuclear physics. The rest of this article will focus on applications in electronic structure theory. Hartree-Fock method calculates the exchange energy exactly, but it does not calculate the effect of electron correlation at all. The correlation energy is a very difficult quantity to calculate. This is because the correlation energy is so directly related to the degrees of freedom in the Hilbert space, which cannot be spanned by the single determinant. The large majority of wave function methods try to span the Hilbert space by introducing multiple Slater determinants and including the unoccupied Hartree-Fock one-electron orbitals in this expansion. The ultimate goal of this would be to give a correct representation of the full electronic wavefunction. The wavefunction in the Born-Oppenheimer approximation is a $3N$ dimensional complex function with N spin coordinates, where N is the number of electrons. The multi-dimensional search of such a wavefunction is prohibitively expensive from a computational point of view for even very small systems. This is the motivation for looking at density functional theory.

4.10.2 Density Functional Theory

Density functional theory (DFT) is an alternative type of *ab initio* method. In physics and chemistry, this method is a quantum mechanical theory used to investigate the electronic structure (principally the ground state) of many body systems, particularly atoms, molecules and the condensed phases and which is the spatially dependent electron density. The success of density functional theory not only encompasses standard bulk materials but also complex materials such as proteins. The main idea of DFT is to describe an interacting system of fermions via its density and not via its many-body wave function. For N electrons in a solid, which obey the Pauli principle and repulse each other via the Coulomb potential, this means that the basic variable of the system depends only on the three spatial coordinates x, y, and z rather than $3N$ degrees of freedom. Density

Functional (DF) techniques are based on two theorems, proved by Hohenberg and Kohn in 1964 [93], and on a computational scheme proposed by Kohn and Sham (KS) the following years [94]. They showed that the total energy is a functional of the electron density. This means that one does not need to know the complicated many-electron wave function; but only the electron density $\rho(\boldsymbol{r})$, which is the key quantity in density functional theory.

$$E^{DFT} = \int_{UNITCELL} \varepsilon^{DFT}(\boldsymbol{r})d\boldsymbol{r} \tag{4.4}$$

Where ε^{DFT} is the DFT energy density, representing exchange-correlation interaction. The ground stats properties of a system of electrons and ions are determined by calculating GS energy from the electron density.

4.10.2.1 Local Density Approximation

Local-density approximations (LDA) are a class of approximations to the exchange-correlation (XC) energy functional in density functional theory (DFT) that depend solely upon the value of the electronic density at each point in space (and not, for example, derivatives of the density or the Kohn-Sham orbital's). Many approaches can yield local approximations to the XC energy. Overwhelming, however, successful local approximations are those that have been derived from the homogeneous electron gas (HEG) model. In this regard, LDA is generally synonymous with functional based on the HEG approximation, which are then applied to realistic systems (molecules and solids). The LDA states that, for regions of a material where the charge density is slowly varying, the exchange correlation energy at that point can be considered the same as that for a locally uniform electron gas of the same charge density in the case we can write E_{xc} as,

$$E_{xc}^{LDA}[\rho] = \int \rho(\boldsymbol{r})\varepsilon_{xc}[\rho(\boldsymbol{r})]d\boldsymbol{r} \tag{4.5}$$

Kohn and Sham [17] give this expression of exchange correlation energy. They also introduced the local spin density approximation (LSDA) where the spin polarization is allowed and the exchange correlation energy becomes a functional of the local electron-spin densities, $\rho\uparrow$ and $\rho\downarrow$:

$$E_{xc}^{LSDA}[\rho\uparrow, \rho\downarrow] = \int \rho(\boldsymbol{r})\varepsilon_{xc}[\rho\uparrow(\boldsymbol{r}), \rho\downarrow(\boldsymbol{r})]d\boldsymbol{r} \tag{4.6}$$

By writing the total energy E_{tot} in this form and applying the variational principle one-electron KS equations may be derived in the following form:

$$\left\{-\frac{1}{2}\nabla^2 + V_{ext}(\boldsymbol{r}) + V_c[\rho(r)] + \mu_{xc}[\rho(\boldsymbol{r})]\right\}\psi_i(\boldsymbol{r}) = \varepsilon_i\psi(\boldsymbol{r}) \tag{4.7}$$

Where, $\mu_{xc}[\rho(\boldsymbol{r})] = \frac{\partial E_{xc}[\rho]}{\partial \rho(\boldsymbol{r})}$

The exchange-correlation energy is decomposed in to exchange and correlation terms linearly,

$$E_{xc} = E_x + E_c \tag{4.8}$$

So that separate expressions for E_x and E_{co} are sought. The exchange term takes on a simple analytic form for the HEG [95].

LDA depends only upon the value of electron density but not on the gradient of electron density. Although this approximation is extremely simple, it is surprisingly accurate, and forms the core of most modern DFT codes. It even works reasonably well in systems where the charge density is rapidly varying. However, it tends to under predict the atomic ground state energies and ionization energies, while over predicting binding energies. It is also known to favour high spin state structures. For these reasons there have been attempts to move beyond the LDA, notably through the addition of gradient corrections to incorporate longer range gradient effects [96]. However, in practice, although these improvements seem to give better total energies the resultant structure is often worse, and at a greatly increased computational cost. In general, the LDA is worse for small molecules and improves with system size.

4.10.2.4 Generalized Gradient Approximation (GGA)

The generalized gradient approximation (GGA) for the exchange functional in conjunction with accurate expressions for the correlation functional have led to numerous applications in which density-functional theory (DFT) provides structures, bond energies, and reaction activation energies in excellent agreement with the most accurate *ab initio* calculations and with the experiment. Many modern codes using DFT now use more advanced approximations to improve accuracy for certain physical properties. The DFT calculations in this study have been made using the Generalized Gradient Approximation (GGA). The generalized gradient approximation (GGA) is more efficient than local density approximation. As stated above, the LDA uses the exchange-correlation energy for the uniform electron gas at every point in the system regardless of the homogeneity of the real charge density. For non-uniform charge densities, the exchange-correlation energy can deviate significantly from the uniform result. This deviation can be expressed in terms of the gradient and higher spatial derivatives of the total charge density. The GGA uses the gradient of the charge density to correct for this

deviation. For systems where the charge density is slowly varying, the GGA has proved to be an improvement over LDA. It is also applicable to the system of inhomogeneous electron gas. Thus it is able to yield the more appropriate results and the exchange-correlation energy E_{xc} is a function of the spin density and their gradients [96]:

$$E_{xc}^{GGA}[\rho\uparrow,\rho\downarrow] = \int [\rho\uparrow(\boldsymbol{r}),\rho\downarrow(\boldsymbol{r}),\nabla\rho\uparrow(\boldsymbol{r}),\nabla\rho\downarrow(\boldsymbol{r})]\, d\boldsymbol{r} \qquad (4.9)$$

The purpose of introduction of GGA is to improve the quality of LDA results significantly.

4.11 Pseudopotentials

The pseudopotential is an attempt to replace the complicated effects of the motion of the core (i.e., non-valence) electrons of an atom and its nucleus with an effective potential, or pseudopotential, so that the Schrödinger equation contains a modified effective potential term instead of the Columbic potential term for core electrons normally found in the Schrödinger equation. The pseudopotential approximation was first introduced by Hans Hellmann in the 1930s. If all of the electrons in a system were explicitly included when performing a calculation and constructed from the full Columbic potential of the nuclei, the computational cost would still be prohibitive using a plane wave basis set. The rapid oscillations of the wavefunctions near to the nucleus, due to the very strong potential in the region and the orthogonality condition between different states, mean that a very large cut-off energy, and hence basis set, would be necessary. Fortunately, the study of Physics and Chemistry shows that the core electrons on different atoms are

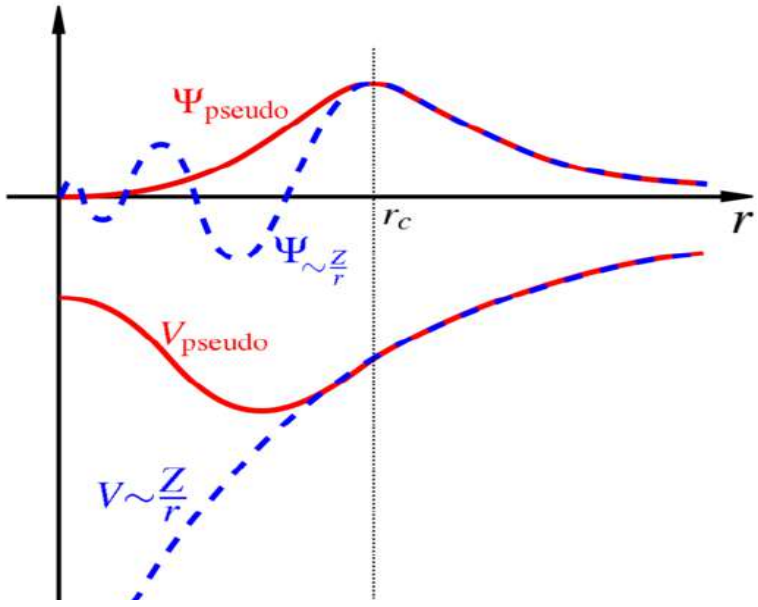

Figure 4.1 A schematic illustration of all-electron (blue lines) and pseudo-potentials (red lines) and their corresponding wavefunctions. The radius at which all-electron and pseudopotential values match is $\boldsymbol{r}_c$.

almost independent of the environment surrounding the atom and that only the valence electrons participate strongly in interactions between atoms. Thus, the core electron states may be assumed to be fixed and pseudopotential may be constructed for each atomic species which takes into account the effects of the nucleus and core electrons. The pseudo wavefunctions corresponding to this modified potential do not exhibit the rapid oscillations of the true wavefunctions, dramatically reducing the number of plane waves needed for their representation. The calculations then need only explicitly consider the valence electrons, offering a further saving in effort. There are two types of Pseudopotentials:

1. Norm-conserving Pseudopotential
2. Ultra-soft Pseudopotential

A pseudopotential is constructed such that it matches the true potential outside a given radius, designated the core radius. Similarly, each pseudo wavefunction must match the corresponding true wavefunction beyond this distance. In addition, the charge densities obtained outside the core region must be identical to the true charge density. Thus, the integral of the squared amplitudes of the real and pseudo wavefunctions over the core region must be identical. This condition is known as norm-conservation [97]. The atomic properties of the element must be preserved, including phase shifts on scattering across the core. These phase shifts will be different for different angular momentum states and so, in general, pseudopotential must be non-local, with projectors for different angular momentum components. The pseudopotential is often represented using the form [98],

$$V = V_{loc} + \sum_{l,m}(V_l - V_{loc})\boldsymbol{P}_{l,m} \tag{4.10}$$

Where, $\boldsymbol{P}_{l,m}$ are the projectors which project the electronic wavefunctions onto the eigenfunctions of different angular momentum states. The choice of V_{loc} is arbitrary and if it is made equal to one of the V_l this avoids the need for the corresponding set of angular momentum projectors. The evaluation of the non-local potential in reciprocal space requires a computational time which is proportional to the cube of the system size. The projections may instead by carried out in real-space, using the method of King-Smith et al. [98], which reduces the computational cost to the order of the system size squared. Pseudopotentials are constructed using an ab initio procedure. The `true' wavefunctions are calculated for an isolated atom using an all-electron DFT approach. The resulting valence wavefunctions are then modified in the core region to remove the oscillations

while obeying the norm-conservation constraint. The Schrödinger equation is then inverted to find the pseudopotential which will reproduce the pseudo wavefunctions. This procedure produces a pseudopotential which may be transferred between widely varying systems. This contrasts with semi-empirical potentials which are constructed to describe a particular atomic environment and may not be simply transferred to different environments.

4.12 Integration in Reciprocal Space

The integration in reciprocal space is an important aspect of *ab initio* calculation for periodic structures. The problem arises at each stage of the self- consistent procedure, when determining the Fermi energy, ε_F, when reconstructing the one-electron density matrix, and after self-consistency is reached, when calculating the density of states (DOS) and a number of observable quantities [99]. The *P* matrix in direct space is computed following equation

$$P_{3,4}^{n} = 2\int_{BZ} dk\, e^{ik.n} \sum_j \alpha_{3j}^{*}(k)\, \alpha_{4j}(k)\theta\left(\varepsilon_F - \varepsilon_j(k)\right) \qquad (4.11)$$

Where α_{ij} denotes the *i*-th component of the *n*-th eigenvector, θ is the step function, ε_F, the Fermi energy and ε_n, the *n*-th eigen value. The technique adopted to compute ε_F and the ***P*** matrix in the SCF step is described in reference [93]. The Fourier-Legendre technique is used to calculate the total and projected DOS [94]. The integral of total energy and the Fermi energy are evaluated from a certain set of sampling points {k} in the reciprocal space.

4.13 The Role of Symmetry Element in Ab initio Calculation

Translational symmetry allows the factorization of the eigenvalue problem in periodic calculation, because the Bloch functions are a basis for irreducible representations of the translational group. In periodic calculations, point symmetry is exploited to reduce the number of points for which the matrix equations are to be solved. Point symmetry is also explicitly used in the reconstruction of the Hamiltonian, which is totally symmetric with respect to the point group operators of the system.

In the HF-CO-LCAO scheme, the very extensive use of point symmetry allows us to evaluate bioelectronic integrals and monoelectronic integrals with saving factors as large as *h* in the number of bioelectronic integrals to be computed or h^2 in the number of those to be stored for the SCF part of the calculation, where *h* is the order of the point group. The main steps of the procedure [100] can be summarized as follows:

(i) The set of Coulomb and exchange integrals whose *3, 4* indices identify translationally equivalent pairs of AOs, so that the associated element of the density matrix P_{34} is the same, are summed together to give D_{1234} elements:

$$D_{1,2T;3,4Q} = \sum_n \left[\left(\varphi_1^o \varphi_2^g \mid \varphi_3^h \varphi_4^{h+n} \right) - \frac{1}{2} \left(\varphi_1^o \varphi_3^h \mid \varphi_3^g \varphi_4^{h+n} \right) \right] \tag{4.12}$$

(ii) The products of AOs $\varphi_1\varphi_2$ (and $\varphi_3\varphi_4$) are classified in symmetry-related sets; using the fact that Fock matrix is totally symmetric, only those quantities are evaluated whose indices *1, 2* refer to the first member of a symmetry set. The corresponding saving factor is as large as *h*.

(iii) Using the symmetry properties of the density matrix, *D* quantities referring to *3, 4* couples belonging to the same symmetry set (and with the same *1,2g* index) can be combined after multiplication by appropriate symmetry matrices, so that a single quantity for each *3, 4* symmetry set is to be stored, with a saving factor in storage of the order of *h*.

(iv) The symmetry $P_{34}^n = P_{43}^{-n}$ is exploited.

(v) The symmetry $F_{12}^g = F_{21}^{-g}$ is exploited.

4.14 CASTEP Code

CASTEP is a software package which uses density functional theory to provide a good atomic-level description of all manner of materials and molecules. CASTEP can give information about total energies, forces and stresses on an atomic system, as well as calculating optimum geometries, band structures, optical spectra, phonon spectra and much more. It can also perform molecular dynamics simulations. CASTEP was originally created by Prof. M.C. Payne and subsequently developed by various UK academics, primarily from the TCM group in Cambridge. For various technical reasons, it was felt in 1999 that the original code was in need of a total re-design and re-write, and so the CASTEP Development Group was created to do just that, using modern coding styles and Fortran90. CASTEP is marketed commercially by Accelya, along with Materials Studio, their graphical frontend for MS Windows. In the United Kingdom there is an academic distribution, maintained by UKCP. The key features of this new plane-wave code were that it was to be:

- » Designed and specified in advance
- » Portable
- » Parallelized

» Clear, modular structure
» Have the same or better feature set as the old F77 code
» Have the same or better performance as the old F77 code

and the first completed version of the new F90 code was ready in 2001.

Due to the new code design, new methods and technologies are quickly and easily added to CASTEP code has been designed for parallel computers from the very beginning, allowing much larger problems to be tackled.

While is not possible to solve the N-electron Schrödinger equation directly, density functional theory (DFT) [93], [94] gives us, in principle, a method to determine the ground state electronic structure of a system. A brief summary of the methodology for electronic structure calculations as implemented in CASTEP is as follows: a set of one-electron Schrödinger (Kohn-Sham) equations are solved using the plane-wave pseudopotential approach [101]. The wavefunctions are expanded in a plane wave basis set defined by use of periodic boundary conditions and Bloch's Theorem. The electron-ion potential is described by means of *ab initio* pseudopotentials within both norm-conserving [102] and ultrasoft [103] formulations. Direct energy minimization schemes are used to obtain, self-consistently, the electronic wavefunctions and corresponding charge density. In particular the conjugate gradient [101] and density mixing [104], [105] schemes are implemented. Also, the robust electron ensemble DFT [106] approach can be used for systems with partial occupancies (in particular, metals). Although the total energy is the central quantity, the response of that energy to external influences is extremely important and can lead to further direct comparisons with experimental data through the calculation of experimental observables. If we perturb the system in some way then the total energy can be expanded as a perturbation series.

4.14.1 Summary of capabilities

CASTEP is a fully featured first principles code and as such its capabilities are numerous. Aiming to calculate any physical property of the system from first principles, the basic quantity is the total energy from which many other quantities are derived. For example, the derivative of total energy with respect to atomic positions results in the forces and the derivative with respect to cell parameters give stresses. These are then used to perform full geometry optimizations and possibly finite temperature molecular dynamics. Furthermore, symmetry and constraints (both internal and external to the cell)

can be imposed in the calculations, either as defined by the user, or automatically using in-built symmetry detection.

- **Total energies:** Calculation of total energy, forces, stresses, and elastic constants.
- **Electronic structure:** Electronic charge densities, orbital's, electrostatic potentials, band structure, total and partial electronic density of states, Mullikan population analysis, and optical properties (such as reflectivity, absorption, refractive index, and dielectric function), subject to the usual DFT band gap considerations.
- **Geometry:** Optimization of atomic positions and unit cell parameters, either constrained or unconstrained and under external pressure and stresses.
- **Molecular dynamics:** Finite temperature molecular dynamics can be performed under various conditions such as constant temperature, energy, volume, and pressure.
- **Transition states:** The LST/QST methods are used to find transitions states.
- **Phonons:** Using density functional perturbation theory (DFPT), phonon frequencies and eigenvectors are calculated which can be used to give the Gibbs free energy, entropy, enthalpy, Debye temperature, heat capacity, and a measurement of phase stability.
- **Electric field response:** DFPT is used to calculate the response of the system of an external electric field yielding bulk polarizabilities, dielectric constants, born effective charges, LO/TO phonon splitting and the IR intensity of phonon modes.
- **Exchange and correlation:** The well-known LDA and GGA functionals are included (such as the PW91, PBE and RPBE functionals), however non-local functionals such as the weighted density approximation (WDA), Hartree-Fock and exact/screened exchange are also available.

CHAPTER -5

CALCULATIONS OF DIFFERENT PROPERTIES OF $TlBO_3$(B = Cr, Mn)

5.1 Introduction

The theoretical explanation of the structural, elastic, electronic and optical properties of $TlCrO_3$ and $TlMnO_3$ are presented in this chapter. The main purpose of this chapter is to provide an overview of the computational tools. All these computational tools are required to completely analyse and explain a compound.

5.2 Computation of Different Properties of $TlBO_3$(B = Cr, Mn)

The investigation of $TlBO_3$(B= Cr, Mn) is done with the most commonly used first-principle modelling of structural, electronic, and optical properties Density Functional Theory (DFT) with the periodic ambient condition along with generalized gradient approximation (GGA) and Perdew-Burke-Ernzerhof (PBE) exchange-correlation functional [73]–[75] using the Cambridge Serial Total Energy Package (CASTEP) code [76]. The atomic calculations for Tl – $6s^2 6p^1$, Cr – $3d^5 4s^1$, Mn – $3d^5 4s^2$ and O – $2s^2 2p^6$ are executed. The Brillouin zone *k*-points sampling is taken using the Monk-horst-Pack scheme [77] with 10 × 7 × 10 grid points for $TlCrO_3$ and 7 × 5 × 7 grid points for $TlMnO_3$. The plane-wave Cut-off energy is 450eV and 400eV for $TlCrO_3$ and $TlMnO_3$ respectively. The Broyden-Fletcher- Goldfarb-Shanno (BFGS) minimization method also known as the quasi-Newton method [78] is employed as a method of optimization of the crystal. The principles of convergence for the optimization are set to 1×10^{-5}eV per atom for total energy, 0.03 eV/Å for maximum force, and 0.05 GPa for maximum stress. The stress-strain method [79] is used to attain the elastic stiffness constants of $TlBO_3$(B= Cr, Mn) using CASTEP. The Yong's modulus, shear modulus along with Poisson's ratio presented in the 3D anisotropy models are obtained using the ELATE program [80]. Lastly, the electronics properties are evaluated by setting the above-mentioned parameters.

5.2.1 Geometry Optimization

Geometry optimization is very significant to find the configuration of minimum energy of the molecule in CASTEP. Geometry optimization of a molecule determines many of its physical and chemical properties. Therefore, understanding of geometry optimization

is essential when running computations. In computational research, we are precisely concerned with optimizing:

- bond angles (degrees)
- bond distances (angstroms)
- dihedral angles (degrees).

Geometry optimization is used to find minima on the potential energy surface, with these minimum energy structures on behalf of equilibrium structures. Optimization is used to locate transition structures, which are represented by saddle points on the potential energy surface. Optimization to minima is also referred to as energy minimization. During minimization, the energy of molecules is reduced by adjusting atomic coordinates. Energy minimization is done when using both molecular mechanics or quantum mechanics methods and it must precede any computational analyses in which these methods are applied.

For example, geometry optimization can be used to

- characterize a potential energy surface
- obtain a structure for a single-point quantum mechanical calculation, which provides a large set of structural and electronic properties
- prepare a structure for molecular dynamics simulation− if the forces on atoms are too large; the integration algorithm may fail.

5.2.2 Electronic Properties

In solid-state physics, the electronic band structure (or simply band structure) of a solid describes those ranges of energy an electron is "forbidden" or "allowed" to have. Band structure derives from the diffraction of the quantum mechanical electron waves in a periodic crystal lattice with a specific crystal system and Bravais lattice. The band structure of a material determines several characteristics, in particular the material's electronic and optical properties.

The band structure diagram contains information about both the bonding interactions within a molecule (intermolecular) and the intermolecular interactions. The band gap is one of the most useful aspects of the band structure, as it strongly influences the electrical and optical properties of the material and stability of a compound toward oxidation or reduction (doping). Electrons can transfer from one band to the other by means of carrier generation and recombination processes. The band gap and defect states created in the band gap by doping can be used to create semiconductor devices such as solar cells,

diodes, transistors, laser diodes and others. Furthermore, the band structure depends on the energy levels of the constituent atomic orbitals and the crystal structure.

Every state in the Brillouin zone (BZ) is characterized by a wave number (k). This wave number is very closely packed within the Brillouin zone for a large crystal. The lowest lying state of a given wave number is called the first band; next lying state of the same given wave number is called the second band and so on. Thus, each of the electronic state is specified by giving its wave number and its band index. Of course, each state has a well-defined energy. Thus, the energy of the nth band will be represented by E_n(k) which turns out to be a quasi-continuous function of wave number for each band, as it was in the case of one dimension. For a large crystal, the function becomes very nearly continuous when the wave numbers allowed by the periodic boundary conditions are very closely spaced. The set of functions E_n (k) is known as the energy band structure.

We already mentioned that DFT method has been used to calculate the band structure of $SrRh_2$. The spectrum of the energy eigen values of a periodic system is the band structure. So, the lattice periodicity of a crystal has important consequences for the dynamic of the electrons. Each level of the isolated atom spreads out to form a band of allowed electron energies. The electronic band structure determines the electronic properties of the crystal.

5.2.3 Density of states (DOS)

In solid-state and condensed matter physics, the density of states (DOS) of a system describes the number of states per interval of energy at each energy level that are available to be occupied. Unlike isolated systems, like atoms or molecules in gas phase, the density distributions are not discrete like a spectral density but continuous. A high DOS at a specific energy level means that there are many states available for occupation. A DOS of zero means that no states can be occupied at that energy level. In general, a DOS is an average over the space and time domains occupied by the system. Local variations, most often due to distortions of the original system, are often called local density of states (LDOS). If the DOS of an undisturbed system is zero, the LDOS can locally be non-zero due to the presence of a local potential.

In order to determine the actual number of electrons in a given energy state, it is necessary to know the number of states in the system which have the energy under consideration multiplied by the probability distribution function. Therefore, if $g\ \varepsilon\ d\varepsilon$ is the number of available quantum states in the energy range ε and $\varepsilon + d\varepsilon$, and F (ε) is the probability function of the electrons occupying a particular energy state ε , then the actual number

of electrons present in the so-called free state in the above energy range at any temperature is given by

$$(\mathcal{E})d\mathcal{E} = (\mathcal{E})\ (\mathcal{E})\mathcal{E} \tag{5.1}$$

Where, the quantity g (ε) is called density of states. Of course, the classical values of g (ε) will be different from the quantum values. Generally, the density of states (DOS) is the spectrum of the number of energy levels per eV versus energy. The electronic density of states is treated as a qualitative instrument for understanding the electronic structure of any material. Especially it is very useful in the point of view of the partial density of states (PDOS). According to PDOS, the states are attributed to the basic functions and then to the atoms of the unit cell. The total DOS is then written as a sum over the atomic contributions. The DOS is calculated by using the expression [107]:

$$n(\varepsilon) = 2\sum_{n,k}\delta(\varepsilon - \varepsilon_n^k) = \frac{2}{V_{BZ}}\Sigma\int \delta(\varepsilon - \varepsilon_n^k)dk \tag{5.2}$$

Where δ is the Dirac delta function and the k is integral extends over the BZ.

The number of electrons in the unit cell is given by, $\int_{-\infty}^{\varepsilon_F} \mathrm{n}(\varepsilon)\ \mathrm{d}\varepsilon$.

5.2.4 Elastic Constant (C_{ij})

The stress required to maintain a given deformation is known as elastic constant of a given material. Both stress and strain have three tensile and three shear components, giving six components in total. The linear elastic stiffnesses C_{ij} form thus a 6x6 symmetric matrix with a maximum of 27 different components, such that $\sigma_i = C_{ij}\varepsilon_j$ for small stresses and strains [108]. Any symmetry present in the structure may make some of these components equal and may let other components vanish. The independent elastic constants are also defined as the second derivatives of the ground state energy with respect to strain components ($\partial\varepsilon_i$) Mathematically it can be generally written as

$$C_{ij} = \frac{1}{V}\left(\frac{\partial^2 E}{\partial\varepsilon_i\partial\varepsilon_j}\right) \tag{5.3}$$

Where, E and V are the energy and volume of the unit cell respectively.

It is not necessary to perform geometry optimization before calculating elastic constants, so we can generate C_{ij} data for the experimentally observed structure. However, more consistent results are obtained if we perform full geometry optimization, including cell optimization and then calculate the elastic constants for the structure which corresponds

to the theoretical ground state. There are three independent components of the elasticity tensor for Cubic $SrRh_2$. Both structures have three different symmetry elements (C_{11}, C_{12} and C_{44}), each of which represents elastic constants ($C_{11} = C_{22}=C_{33}$; $C_{12} = C_{21}$, $C_{12}= C_{23} = C_{31}$; $C_{44} = C_{55}$ and C_{66}). Methods to determine the elastic constants from first-principles usually involve setting either the stress or strain to a finite volume, re-optimizing any free parameters and calculating the other property (the strain or stress, respectively). By careful choosing the applied deformation, elastic constants can then be determined. However, applying a given homogeneous deformation (strain) and calculating the resulting stress usually requires far less computation effort, since the unit cell is fixed and does not require optimization. This is the method in CASTEP [81].

5.2.5 Optical Properties

The calculation of optical spectra involves not only the occupied and unoccupied states of the electronic structure but also the character of the bands. Hence, it is interesting to study the optical properties to have more insight into the electronic structure of materials. Further, the comparison of the calculated optical spectra with experimental measurements is the best way to check the calculated electronic structure. The dielectric function [$\varepsilon(\omega) = \varepsilon_1(\omega) + i\varepsilon_2(\omega)$] is known to describe the optical response of the medium at all photon energies $E = \hbar\omega$. The imaginary part of the dielectric $\varepsilon_2(\omega)$ is calculated by summing transitions from occupied to unoccupied states. Specifically, in this study, the imaginary part of the dielectric function $\varepsilon_2(\omega)$ is given as in [109] by

$$\varepsilon_2(\omega) = \frac{2e^2\pi}{\Omega\varepsilon_0}\sum_{k,v,c}|\psi_k^c|u.r|\psi_k^v|^2\,\delta(E_k^c - E_k^v - \hbar\omega) \tag{5.4}$$

The real part of the dielectric function can be extracted from the imaginary part using the Kramers-Kronig relation in the form [110], [111]

$$\varepsilon_2(\omega) = 1 + \frac{2}{\pi}P\int_0^\infty \frac{\omega'\varepsilon_2(\omega')d\omega'}{(\omega'^2-\omega^2)} \tag{5.5}$$

Where, P implies the principal value of the integral.

The knowledge of both the real and imaginary parts of the dielectric tensor allow the calculation of important optical functions. In this study, we present and analyse the reflectivity $R(\omega)$, the absorption coefficient $I(\omega)$, the optical conductivity $\sigma(\varepsilon)$, the electron energy loss spectrum $L(\omega)$, as well as the refractive index $n(\omega)$ and the extinction coefficient $k(\omega)$. The reflectivity spectra are derived from Fresnel's formula for normal

incidence assuming an orientation of the crystal surface parallel to the optical axis using the relation [112]

$$R(\omega) = \left| \frac{\sqrt{\varepsilon(\omega)}-1}{\sqrt{\varepsilon(\omega)}+1} \right|^2 \tag{5.6}$$

Arising from $\varepsilon_1(\omega)$ and $\varepsilon_2(\omega)$, all the other optical properties, such as reflectivity *R(ω)*, absorption coefficient *I(ω)*, refractive index *n(ω)*, and energy-loss spectrum *L(ω)* can be calculated [112], [113]:

$$R(\omega) = \left| \frac{\sqrt{\sqrt{\varepsilon_1(\omega)+j\varepsilon_2(\omega)}-1}}{\sqrt{\sqrt{\varepsilon_1(\omega)+j\varepsilon_2(\omega)}+1}} \right|^2 \tag{5.7}$$

$$I(\omega) = \sqrt{2}(\omega)\left\{\sqrt{\varepsilon_1(\omega)^2+\varepsilon_2(\omega)^2}-\varepsilon_1(\omega)\right\}^{1/2} \tag{5.8}$$

$$n(\omega) = \left[\frac{\varepsilon_1(w)}{2} + \frac{\sqrt{\varepsilon_1(\omega)^2+\varepsilon_2(\omega)^2}}{2}\right]^{1/2} \tag{5.9}$$

$$L(\omega) = \frac{\varepsilon_2(\omega)}{\varepsilon_1(\omega)^2+\varepsilon_2(\omega)^2} \tag{5.10}$$

The optical spectra such as the extinction coefficient, *k(ω)*, is easily calculated in terms of the components of the complex dielectric function as follows.

$$k(\omega) = \left[\frac{\sqrt{\varepsilon_1(\omega)^2+\varepsilon_2(\omega)^2}}{2} - \frac{\varepsilon_1(w)}{2}\right]^{1/2} \tag{5.11}$$

CHAPTER-6

RESULTS AND DISCUSSION

6.1 Introduction

The results of the study of different physical properties of $TlBO_3$(B = Cr, Mn) are presented in this chapter. The structural properties, e.g., optimized lattice parameters, equilibrium volume and internal parameter are reported and analysed. We determine different elastic properties such as bulk modulus, shear modulus, young's modulus, Poisson's ratio, compressibility and the independent elastic constants of both $TlCrO_3$ and $TlMnO_3$. The electronic band structures and the total and partial densities of states (DOSs) at zero pressures are calculated and analysed. We also study different optical properties which include dielectric function, refractive index, Reflectivity, absorption coefficient, energy loss function and conductivity as a function of photon energy along [100] directions. Electronics properties, Vickers Hardness, and thermodynamic properties are also determined All these results are analysed with suitable figures and compared with available theoretical and experimental data with satisfactory agreements.

6.2. Structural properties

$TlBO_3$(B=Cr, Mn) perovskite materials prepared with stoichiometric mixtures of Cr_2O_3(for $TlCrO_3$), Fe_2O_3(for $TlMnO_3$) and Tl_2O_3 [36], [54]. Both materials share the same $TlBO_3$ ionic structure but both share different crystal structure types. **Figure 6.1** and **Figure 6.2** illustrates the Crystal structure of $TlBO_3$(B = Cr, Mn). $TlCrO_3$ crystalizes in orthorhombic structure by means of space group Pnma (no. 62). In $TlCrO_3$ for Tl site 4c Wyckoff position (0.04617, 0.25, 0.98732), Cr site 4b Wyckoff position (0, 0, 1/2) and for O there are two site, for the first one 4c Wyckoff position (0.4504, 0.25, 0.1050) and for the second 8d Wyckoff position (03009, 0.0558, 0.6969) [36]. $TlMnO_3$ crystalizes in triclinic structure with space group $P\bar{1}$(no. 2). In $TlMnO_3$, Tl site has 2*i* (0.54745, 0.25794, 0.50994) and 2*i* (0.04935, 0.24233, 0.97513). For Mn atoms are positioned in 4 sites. Mn1, Mn2, Mn3 and Mn4 has 1*d* (1, 0.5, 0, 0); 1e (1, 0.5, 0.5, 0); 1*b* (1, 0, 0, 0.5); 1*g* (1, 0, 0.5, 0.5) respectively. O atoms are positioned in 6 site O(1-6) which are in numerical order as follows, 2*i* (for all sites) Wyckoff position (0.9423, 0.2309, 0.3799); (0.4450, 0.2708, 0.1147); (0.2056, 0.5732, 0.2055); (0.8053, 0.0511, 0.8070); (0.2824, 0.4406, 0.6847); (0.6839, 0.9275, 0.2855) respectively [54]. The optimized lattice parameters a, b and c are presented in **Table 6.1** along with calculated

unite cell volume V. The obtained results are associated with former results and seems to be in good amenability with those outcomes, which indicates our calculations to be reliable. Both materials share different crystals structures, but the calculated lattice constants are pretty close. The Volume for both $TlCrO_3$ and $TlMnO_3$ are calculated and seems to have near lattice constant values.

Table 6.1 Calculated lattice constants and unit cell volume of $TlBO_3$ (B = Cr, Mn).

Compound	Lattice constants (Å)			Volume ($Å^3$)	Remarks
	a	b	c		
$TlCrO_3$ (Orthorhombic)	5.433306	7.693412	5.434486	227.16511	This work.
	5.40318	7.64699	5.30196	219.06671	Exp[36]
	5.405	7.647	5.302	219.14245	Exp[34]
$TlMnO_3$ (Triclinic)	5.457218	7.692286	5.463322	229.341717	This work.
	5.4248	7.9403	5.28650	227.713553	Exp[54]
	5.41987	7.9250	5.27683	226.652881	Exp[55]

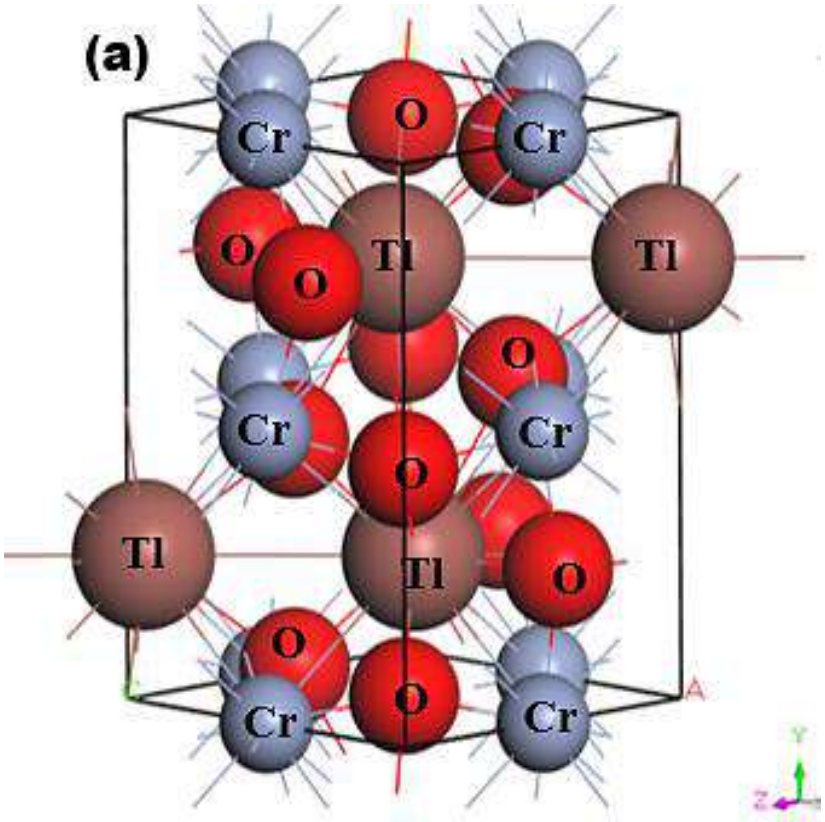

Figure 6.1 Crystal structures of (a) $TlCrO_3$.

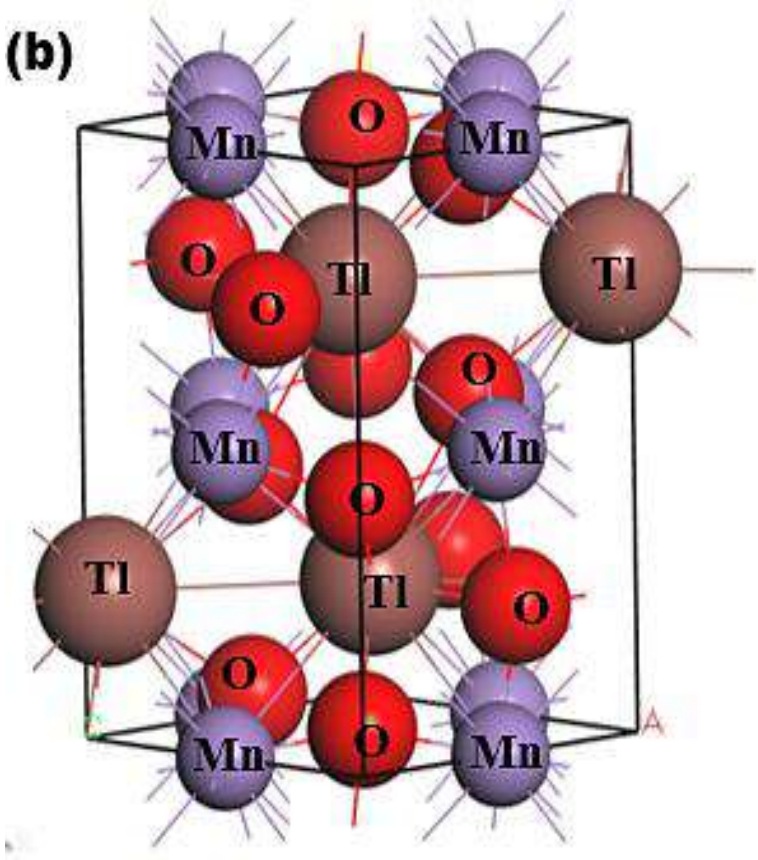

Figure 6.2 Crystal structures of $TlMnO_3$.

6.3 Elastic properties

Elastic characteristics of crystal define various features of solid under symmetry conditions, as well as solid stability, bonding characteristics, elastic, and machinability [114]. The elastic constants are produced from the first approach via the CASTEP module, using a variety of uniform finite value distortions. After optimization of the internal degrees of freedom, the stresses are therefore determined [115]. The elastic constants for $TlBO_3$(B = Cr, Mn) are determined and presented in **Table 6.2**. Nine elastic constants are calculated for orthorhombic $TlCrO_3$ and twenty-one elastic constants are found for triclinic $TlMnO_3$. No past results regarding elastic constants are not found; thus, no relative investigation has been shown. The current outcomes (elastic constants) must mollify the Born stability principles by describing the following relationships:

C_{11}-C_{12} > 0, C_{44} > 0, and C_{11} + 2C_{12} > 0 (6.1)

The elastic constants calculated are positive (**Table 6.2**) and upheld the mentioned stability criteria, which confirms the mechanical stability of $TlBO_3$(B = Cr, Mn). The

material also satisfy generalized stability criteria for orthorhombic crystal ($TlCrO_3$) [76], [116], [117], which is:

$C_{ij} > 0$, (ij = 1-6); (6.2)

$[C_{11}+ C_{22}+ C_{33}+ 2 (C_{12}+ C_{13}+ C_{23})] > 0$; (6.3)

$[C_{11}+ C_{22}- 2C_{12}] > 0$; (6.4)

$[C_{13}+ C_{33}- 2C_{13}] > 0$; (6.5)

$[C_{22}+ C_{33}- 2C_{23}] > 0$; (6.6)

The elastic constants of the compound in **Table 6.2** agreed with the above conditions, further confirming the considered compound $TlCrO_3$ is mechanically stable in the orthorhombic phase. For both materials, the C_{44}, C_{55}, and C_{66} crudely agree with the distortions of the lattice angles (α, β, and γ). It can be concluded that γ is the maximum stable angle owing that the elastic constant C_{66} is bigger than C_{44}/C_{55} (**Table 6.2**), that is dependable on the changing tendencies of lattice angles in the crystal [118]. Here C_{11} is connected with linear compression resistance with the x-direction and the value C_{11} being studied has a higher value than C_{12}, which recommends incompressibility near the a-axis, not near the b-axis. The bond direction of **[100]** is rougher if being compared with the direction of **[011]**. It can also be noticed that the calculated C_{33} of $TlMnO_3$ (**Table 6.2**) is higher than C_{11} and C_{22} for all the compounds, implying that the incompressibility along the c axis is sturdier than near the crystallographic a and b axes. As a result, the bonding strength near the **[001]** direction is greater than that near the **[101]** and **[011]** directions in this compound. From Cauchy pressure ($C_{12} – C_{44}$) the metallic or non-metallic features of the compounds are revealed. The materials will be non-metallic if the Cauchy pressure shown in **Table 6.3** is negative, which is not the case. So, both $TlCrO_3$ and $TlMnO_3$ have metallic nature as the Cauchy pressure values are positive.

Voigt-Reuss-Hill (VRH) approximations are employed to evaluate the polycrystalline elastic properties [119]–[121]. Bulk modulus (B_V) and shear modulus (G_V) in Voigt approximation is expressed as:

$B_V = 1/9\ [(2(C_{11} + C_{12}) + 4\ C_{13} + C_{33})]$; (6.7)

$G_V = 1/30\ (C_{11} + C_{12} - 4C_{13} + 12C_{44} + 12C_{66})$; (6.8)

The Bulk modulus B_R and shear modulus G_R in the Reuss approximation is defined as:

$B_R = \frac{C^2}{M}; \qquad C^2 = (C_{11} + C_{12})C_{33} - 2C_{13}^2;$ (6.9)

$M = C_{11} + C_{12} + 2C_{33} - 4C_{13};$ (6.10)

$$G_R = \frac{1/2[5C^2C_{44}C_{66}]}{3B_vC_{44}C_{66}+C^2(C_{44}+C_{66})}; \qquad C_{66} = \frac{C_{11}-C_{12}}{2}; \tag{6.11}$$

Table 6.2 Elastic constants, C_{ij} (GPa) of $TlBO_3$(B = Cr, Mn).

$TlCrO_3$ (Orthorhombic)		$TlMnO_3$ (Triclinic)			
C_{11}	298.487	C_{11}	247.771	C_{23}	144.011
C_{22}	252.195	C_{22}	219.456	C_{24}	-0.484
C_{33}	298.712	C_{33}	298.029	C_{25}	1.908
C_{44}	104.875	C_{44}	87.156	C_{26}	-1.104
C_{55}	42.099	C_{55}	35.395	C_{34}	-3.159
C_{66}	104.859	C_{66}	74.132	C_{35}	2.344
C_{12}	150.459	C_{12}	131.126	C_{36}	-0.291
C_{13}	85.594	C_{13}	110.109	C_{45}	-1.427
C_{23}	150.071	C_{14}	-6.898	C_{46}	1.183
		C_{15}	0.171	C_{56}	1.436
		C_{16}	-1.434		

B and G is then used to determine the Yong's modulus Y and Poisson's ratio v via the equations:

$$Y = \frac{9BG}{3B+G}; \tag{6.12}$$

$$\nu = \frac{3B-2G}{2(3B+G)}; \tag{6.13}$$

The elastic moduli bulk modulus *B*, shear modulus *G*, Young's modulus *Y*, and Poisson's *v* describes the mechanical performances of solids, that are calculated by VRH approximations [122]–[124]. The VRH scheme is frequently used for evaluating the mechanical behaviours and performances of compounds with elastic constants for a single crystal [125].

$$B = \frac{1}{2}(B_V + B_R); \tag{6.14}$$

$$G = \frac{1}{2}(G_V + G_R); \tag{6.15}$$

The resistance in contradiction to volume, shear, and longitudinal deformation is represented by bulk modulus *B*, shear modulus *G*, and young's modulus *Y* respectively. *Y, G*, and *B* of $TlBO_3$ are determined for the first time in this investigation and shown in **Table 6.3** Pugh's ratio depicted as *B/G* in **Table 6.3** demonstrates if a material is ductile or brittle [126] is more than 1.75, indicating the ductile nature of both materials; otherwise, it behaves brittle in manner. Likewise, Poisson's ratio, v is an additional pointer to anticipate the ductile or brittle manner of solids [127]. The value should be more than 0.25 to be ductile and less to be brittle. As the value of v is more than 0.25 as shown in **Table 6.3** it further confirms the result obtained from Pugh's ratio, suggesting both $TlCrO_3$ and $TlMnO_3$ to be ductile. Furthermore, the value of the Cauchy pressure ($C_{11} - C_{44}$) is positive, indicating the ductile nature of both materials otherwise it would be brittle if the value is negative [128].

Table 6.3 The estimated bulk modulus, B_R(Reuss), B_V(Voigt), *B*(Hill) (GPa), shear modulus, G_R(Reuss), G_V(Voigt), *G*(Hill) (GPa), Young's modulus, *Y*(GPa), Pugh's ratio, *B/G*, Poisson's ratio *v*, Cauchy pressure, C_{12}-C_{44}, and machinability index, μ_M of $TlBO_3$ (B = Cr, Mn).

Elastic moduli and mechanical properties											
Compound	B_R	B_V	B	G_R	G_V	G	Y	B/G	v	C_{12}-C_{44}	μ_M
$TlCrO_3$ (Orthorhombic)	179.9	180.1	180.1	68.4	81.3	74.8	197.1	2.41	0.32	45.6	1.72
$TlMnO_3$ (Triclinic)	168.6	170.6	169.6	56.8	64.7	60.7	162.8	2.79	0.34	43.9	1.93

The machinability index μ_M describes the cutting capability of a compound, the maximum financial level of machine operation, and plastic strain, which is vital for industrial areas. It is determined as follows:

$$\mu_M = \frac{B}{C_{44}}. \tag{6.16}$$

For both orthorhombic $TlCrO_3$ and $TlMnO_3$, the value of μ_M in **Table 6.3** is more than 2, referring to improved lubricating characters and lesser frictions, which has significant applications for different fields.

6.4. Elastic Anisotropy

The microscopic activity of solids is developed by the amount of elastic anisotropy for single and polycrystalline materials[129]. Therefore, the investigation of the outward directional dependence of the elastic tensor is important for the materials involved so that the mechanical resilience, degree of elastic anisotropy, and usage of material under peripheral stress can be heightened. In applied engineering sciences these appearances will equally play a critical part in design activities, clear interpretations, along with fundamental crystal physics[130]. The Shivakumar Ranganathan model represents the elastic anisotropy as[120]:

$$A^U = 5\frac{G_V}{G_R} + \frac{B_V}{B_R} - 6 \geq 0. \tag{6.17}$$

A^U = 0, represents the isotropic performance, although the exemption from this ($A^U \neq 0$) replicates the anisotropic performance of materials. Therefore, the values of A^U are estimated for orthorhombic $TlCrO_3$ (~0.941) and triclinic $TlMnO_3$ (~0.702) characterizing both materials as anisotropic. Furthermore, Chung and Buessum presented the conception of percent anisotropy modulus, A_G (shear), and A_B (bulk) as[119]: (in polycrystalline materials)

$$A_G = \frac{G_V - G_R}{2G_H}; \quad A_B = \frac{B_V - B_R}{B_V + B_R}. \tag{6.18}$$

For A_G = A_B = 0, the solid materials represent the elastic isotropy. So, in the present analysis, both $TlCrO_3$ and $TlMnO_3$ show anisotropic aspects. If we consider the directional requirement on the elastic tensor, $TlMnO_3$ shows a bigger degree of anisotropy. Additionally, shear anisotropy is more prevalent, as it seems to have greater value (**Table 6.4**) for both materials. In both materials $TlBO_3$(B = Cr, Mn) the bulk modulus is anisotropic, as we observed $B_H \neq B_R \neq B_V$. The value of A_B in **Table 6.4** illustrates the bulk modulus of compounds is anisotropic and $TlMnO_3$ is further anisotropic than $TlCrO_3$ which shows negligible anisotropic character. Both compounds indicate anisotropic character (**Table 6.4**) in measured shear anisotropic factors as well. The anisotropic shear pointers offer a valuation of the degree of anisotropy in the bonding of different planes between atoms. Along {100}, {010}, and {001} shear planes the shear anisotropic parameters are stated as:

$$A_1 = \frac{4C_{44}}{C_{11}+C_{33}-2C_{13}};\ A_2 = \frac{4C_{55}}{C_{22}+C_{33}-2C_{23}};\ A_3 = \frac{4C_{66}}{C_{11}+C_{22}-2C_{12}}. \quad (6.19)$$

In the case of $A_1 = A_2 = A_3$, the materials show isotropic nature or else it measures the amount of elastic anisotropy exhibited by the crystal. Since A_1, A_2 and A_3 are not equivalent (**Table 6.4**) both orthorhombic and triclinic materials display anisotropic character. The Zener anisotropy index (A) and the Zener anisotropy equivalent (A^{eq}) for both compounds are calculated to achieve acceptable anisotropy as [131], [132]:

$$A = \frac{2C_{44}}{C_{11}-C_{12}}, \quad (6.20)$$

$$A^{eq} = \left(1 + \frac{5}{12}A^U\right) + \sqrt{\left(1 + \frac{5}{12}A^U\right)^2 - 1}. \quad (6.21)$$

In **Table 6.4** values of A and A^{eq} confirm our previous analysis, reinstating that both compounds have an anisotropic character. The anisotropy index A = 1 suggests the isotropic behaviour of solid materials and anisotropic natures are revealed for more or less than Uni (>1 or <1). The evaluated value of $TlBO_3$(B = Cr, Mn) indicates both materials to be anisotropic where $TlCrO_3$ manifested a slightly higher degree of elastic anisotropy.

Table 6.4 Calculated Shear anisotropic factors, $A_i(i = 1\text{-}3)$, Zener's anisotropy index (A), anisotropy in shear (A_G), anisotropy in bulk modulus (A_B), universal anisotropy index (A^U) and equivalent Zener anisotropy (A^{eq}) of $TlBO_3$ (B = Cr, Mn).

Compound	Crystal system	A_1	A_2	A_3	A	A_G	A_B	A^U	A^{eq}
$TlCrO_3$	Orthorhombic	0.985	0.672	1.679	1.417	0.086	0.0007	0.94	2.360
$TlMnO_3$	Triclinic	1.071	0.617	1.447	1.494	0.065	0.0059	0.70	2.11

To further study the elastic anisotropy of both materials, Young's modulus (Y), bulk modulus (K), shear modulus (G), and Poisson's ratio (v) elastic moduli are constructed for both $TlCrO_3$ and $TlMnO_3$ in **Figure 6.3** and **Figure 6.4** by using ELATE code[80]. The 3D and 2D models are used to identify the nature of anisotropy. If the 3D plots are entirely spherical and their projection on different planes is rounded, the materials are isotropic. The non-spherical shape in the 3D plots for both orthorhombic $TlCrO_3$ and triclinic $TlMnO_3$ signifies the extent of anisotropy.

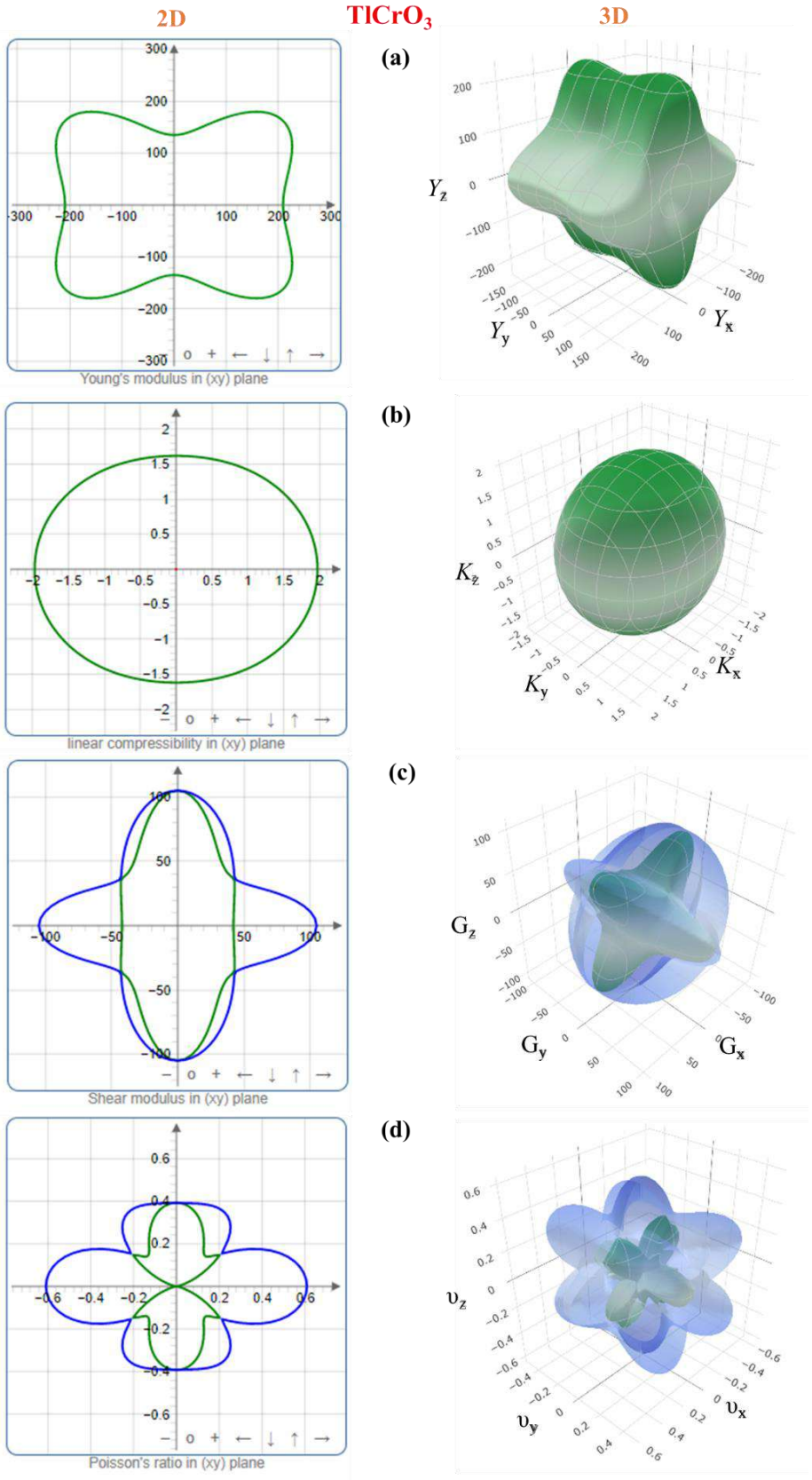

Figure 6.3 3D and 2D anisotropy contour plots of (a)Young's modulus, *Y*, (b)shear modulus, *G*, and (c)Poisson's ratio, *v* of $TlCrO_3$.

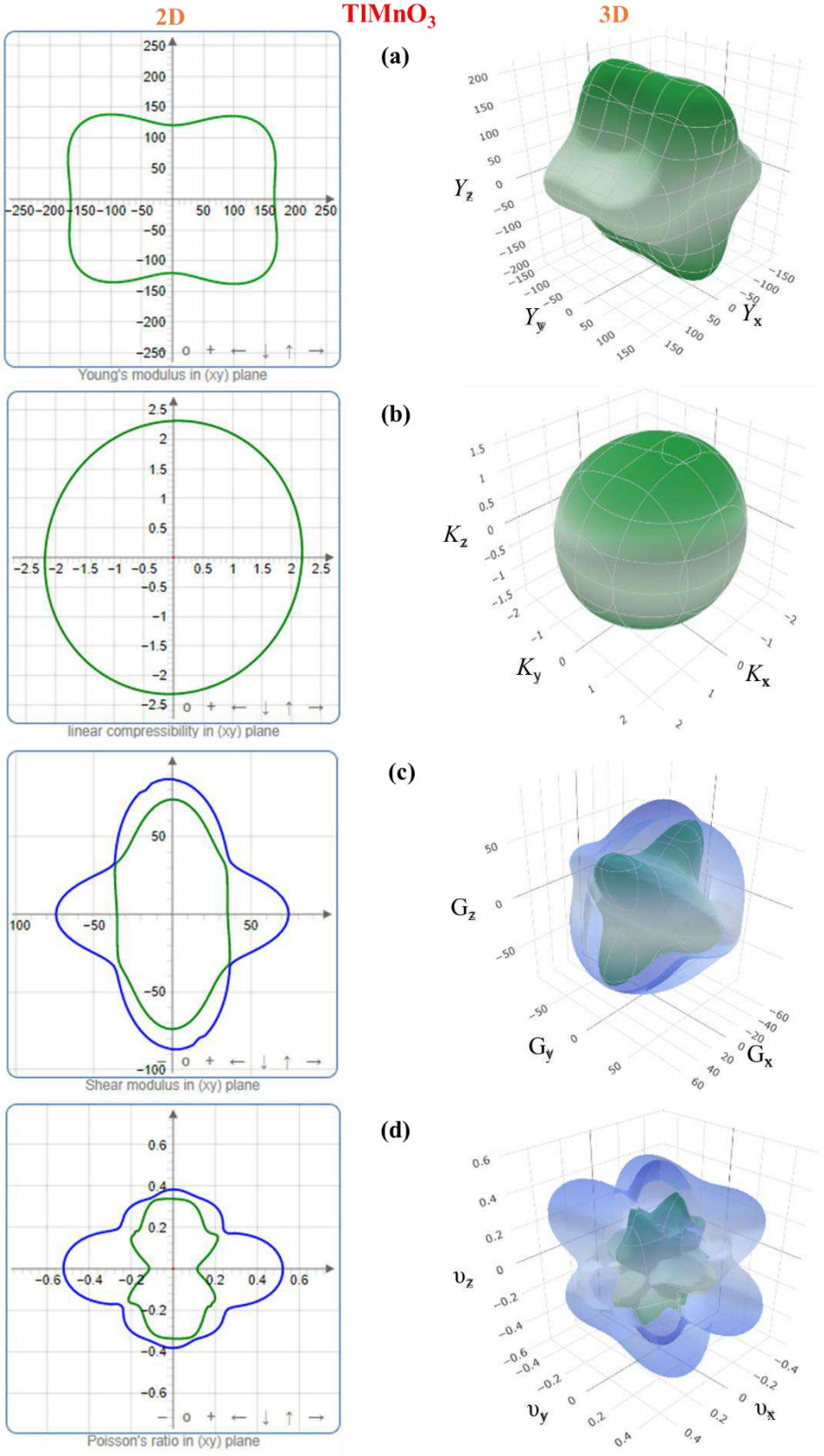

Figure 6.4 3D and 2D anisotropy contour plots of (a)Young's modulus, *Y*, (b)shear modulus, *G*, and (c)Poisson's ratio, *v* of $TlMnO_3$.

As depicted in **Figure 6.3** and **Figure 6.4** the unconventionality between the 3D surface and sphere for all the moduli, suggests the elastic anisotropy characteristics for $TlBO_3$(B = Cr, Mn). This analysis displays good consistency with the results of all the anisotropy indexes discussed above. Along different planes, the anisotropic indices also vary as shown in **Table 6.5** for the assessment of the anisotropic characteristics of mentioned elastic moduli. Furthermore, the 3D plot of different anisotropy moduli looks somewhat similar in **Figure 6.3** and **Figure 6.4** for both compounds.

Table 6.5 The minimum and the maximum values of young's modulus (*Y*), compressibility (*K*), shear modulus (*G*), and Poisson's ratio (*v*) of $TlBO_3$(B = Cr, Mn).

Compound		Y_{min} (GPa)	Y_{max} (GPa)	K_{min} (TPa^{-1})	K_{max} (TPa^{-1})	G_{min} (GPa)	G_{max} (GPa)	v_{min}	v_{max}
$TlCrO_3$ (Orthorhombic)	Value	119.3	264.6	1.617	1.97	42.09	106.5	-0.019	0.66
	Anisotropy	2.217		1.2186		2.53		∞	
$TlMnO_3$ (Triclinic)	Value	104.92	226.94	1.403	2.335	35.25	87.2	-0.030	0.66
	Anisotropy	2.163		1.6643		2.473		21.7979	

6.5. Vickers hardness

Vickers hardness is mainly associated with the resistance offered by the material to plastic deformation. The ability of a material to refuse plastic deformation can also be estimated by it. Many important applications for practical devices can be predicted by understanding the hardness of a solid. Furthermore, a deep understanding of mechanical behavior can be achieved through the relationship between elastic polycrystalline modules and hardness. Vickers hardness can be calculated for metallic compounds by the means of the equation found by Gou et al. [133]. If all the individual bond hardness is calculated, their geometric average can be used to evaluate the hardness of a multiband solid. It can be done by following equations [134]–[136]:

$$H_V = \left[\prod \pi\left(H_v^{\mu}\right)^{n^{\mu}}\right]^{1/\sum n^{\mu}} \tag{6.22}$$

$$H_v^{\mu} = 740(P^{\mu} - P^{\mu\prime})\left(v_b^{\mu}\right)^{-5/3}; \tag{6.23}$$

$$P^{\mu\prime} = \frac{n_{free}}{V}; \tag{6.24}$$

$$n_{free} = \int_{E_P}^{E_F} N(E)dE \tag{6.25}$$

$$v_b^{\mu} = \frac{(d^{\mu})^3}{\sum_v [(d^{\mu})^3 N_b^v]} \tag{6.26}$$

Here, $P^{\mu'}$ and P^{μ} is the Mulliken population and the metallic population of the μ-type bond respectively, n_{free}, is the number of free electrons between the first pseudo gap and Fermi level, V is called cell volume (**Table 6.1**), v_b^{μ}, is the volume of a bond of μ-type, $(d^{\mu})^3$, is the bond length of μ-type bond and N_b^v is the bond number of v per unit volume.

Table 6.6 Theoretical Hardness of $TlBO_3$(B = Cr, Mn)

Compounds	**Bond**	n^{μ}	d^{μ} **(Å)**	P^{μ}	$P^{\mu'}$	v_b^{μ}**(Å³)**	H_v^{μ}**(GPa)**	H_v **(GPa)**
$TlCrO_3$	O-Cr (I)	8	1.9201	0.55	0.043743	9.43794	8.888053	8.72858
	O-Cr (II)	8	1.92232	0.54	0.043743	9.47072	8.662297	
	O-Cr (III)	8	1.92342	0.54	0.043743	9.48698	8.637555	
$TlMnO_3$	O-Mn(I)	2	1.95981	0.36	0.071407	5.04956	14.36908	5.20793
	O-Mn (II)	2	1.96337	0.36	0.071407	5.07713	14.23928	
	O-Mn (III)	2	1.96358	0.36	0.071407	5.07876	14.23167	
	O-Mn (IV)	2	1.96733	0.35	0.071407	5.10791	13.60809	
	O-Mn (V)	2	1.9818	0.35	0.071407	5.22145	13.1185	
	O-Mn (VI)	2	1.98243	0.35	0.071407	5.22643	13.09767	
	O-Mn (VII)	2	1.98378	0.35	0.071407	5.23711	13.05316	
	O-Mn (VIII)	2	1.98532	0.34	0.071407	5.24932	12.53589	
	O-Mn (IX)	2	1.98597	0.32	0.071407	5.25448	11.58347	
	O-Mn (X)	2	1.98904	0.32	0.071407	5.27888	11.49435	
	O-Mn (XI)	2	1.99018	0.35	0.071407	5.28797	12.84463	
	O-Mn (XII)	2	1.99083	0.34	0.071407	5.29315	12.36337	
	O-Tl (I)	2	2.28171	0.1	0.071407	7.9688	0.665542	
	O-Tl (II)	2	2.30589	0.1	0.071407	8.22484	0.631371	
	O-Tl (III)	2	2.33132	0.14	0.071407	8.49997	1.433789	
	O-Tl (IV)	2	2.36947	0.12	0.071407	8.92412	0.936555	
	O-Tl (V)	2	2.39337	0.12	0.071407	9.19689	0.890718	
	O-Tl (VI)	2	2.41888	0.11	0.071407	9.49411	0.670893	

The evaluated values of Vickers hardness of $TlBO_3$(B = Cr, Mn) are displayed in **Table 6.6**. It is clear from **Table 6.6** that $TlCrO_3$ is harder than $TlMnO_3$. However, overall observation of the values reveals both materials to have lower hardness compared to diamond considered the most rigid (Vickers hardness 70 to 150 GPa) [137] material among all. As a result, both $TlCrO_3$ and $TlMnO_3$ indicate flexible and soft nature, making them suitable for thin-film production. The hardness values are 8.729 GPa for $TlCrO_3$ and 5.208 GPa for $TlMnO_3$ which is close to 2 – 8 GPa, values of many well-known MAX phases (M is transition metal, A is group 13–15 A element, X is C or N) materials [138].

6.6. Electronic properties

The electronic properties of the $TlBO_3$(B = Cr, Mn) perovskites are studied by measuring the band structure and along with the total partial density of states (DOS). The electronic band structures for both orthorhombic $TlCrO_3$ and triclinic $TlMnO_3$ are displayed in **Figure 6.5** and **Figure 6.6** correspondingly.

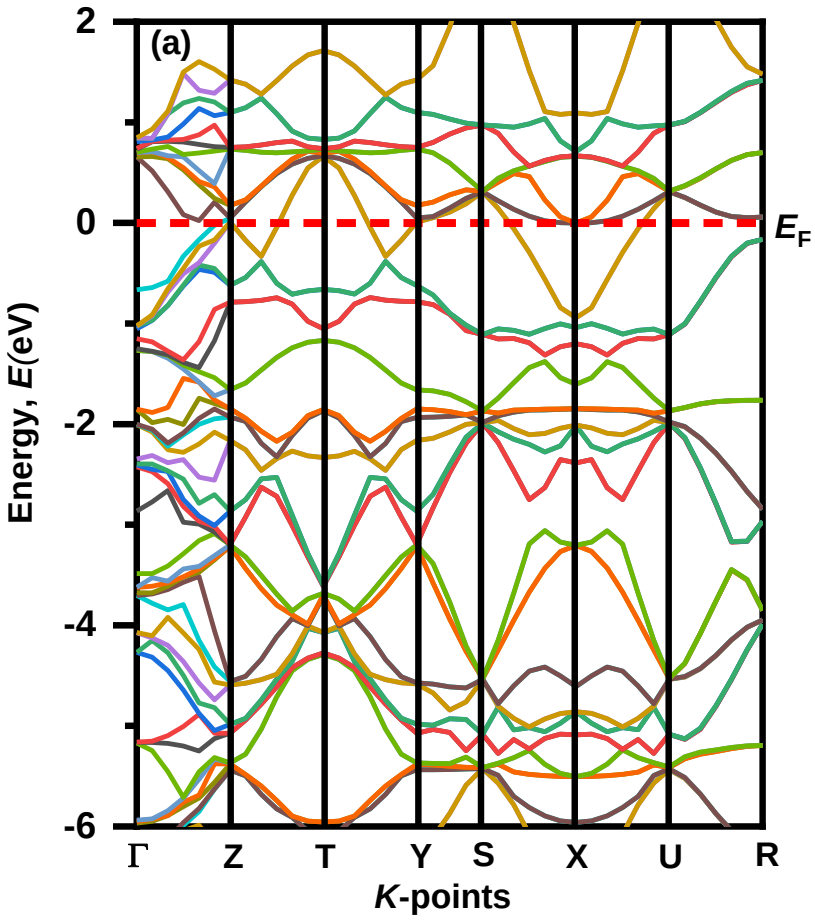

Figure 6.5 Electronic band structure of (a) $TlCrO_3$ and (b) $TlMnO_3$.

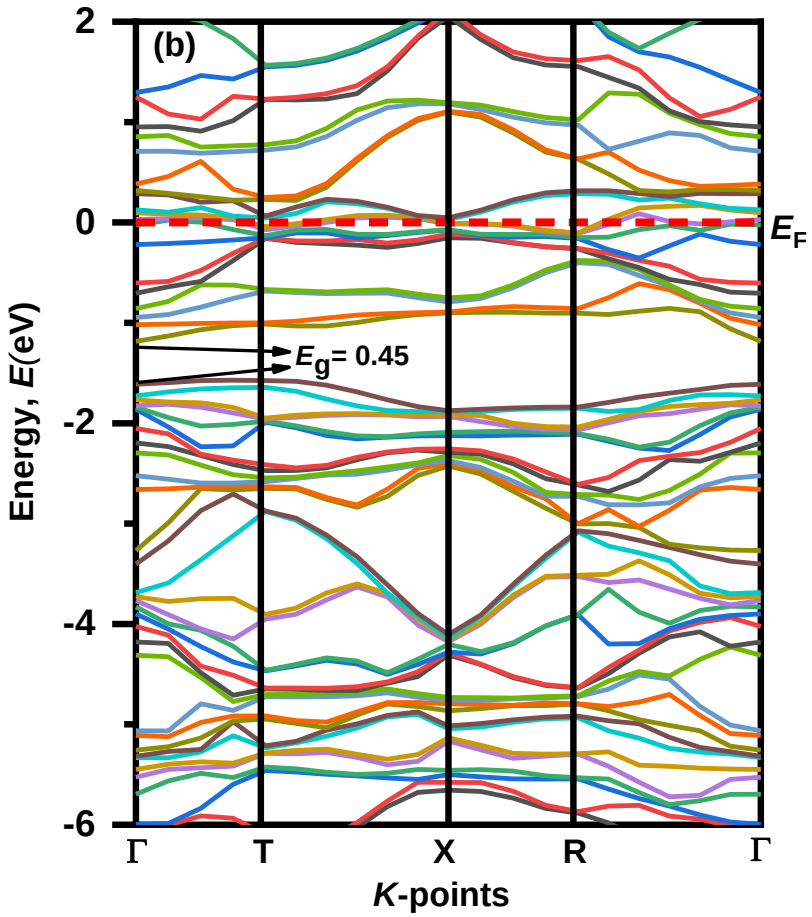

Figure 6.6 Electronic band structure of $TlMnO_3$

The straight (dotted) line at 0 eV specifies the Fermi level (E_F) separating the conduction band and the valence band. For both materials energy bands with bulky scattering diagonally the Fermi level (E_F), the conduction and valence bands both are superimposed and displayed no bandgap, suggesting both materials to be metals. Moreover, the energy density of $TlMnO_3$ along the Fermi level (E_F) describes it to be more metallic than $TlCrO_3$. The bandgap (E_g = 0.45) in **Figure 6.6** reveals possible semiconducting abilities in $TlMnO_3$. No previous study on the density of states and band structure is done. The evaluated total (TDOS) and partial density of states (PDOS) with atomic contributions of different orbitals around E_F by CASTEP code are displayed in **Figure 6.7** and **Figure 6.8** for $TlCrO_3$ and $TlMnO_3$ respectively. At E_F the TDOS values are 20 and 24 states/eV give or take for $TlCrO_3$ and $TlMnO_3$ respectively. For both materials, the Tl-3*p* orbital seems to be contributing to both the valence band and conduction band. $TlCrO_3$ contributing for both bands at ~ -0.7eV (~3.3 states/eV) and ~0.13eV (3.7 states/eV). $TlMnO_3$ contributing at ~ -0.6eV (~1.7 states/eV) and ~1.6eV (~2.4 states/eV). $TlCrO_3$

contributes more to the formation of both conduction and valence bands, resulting in less overlap of both bands.

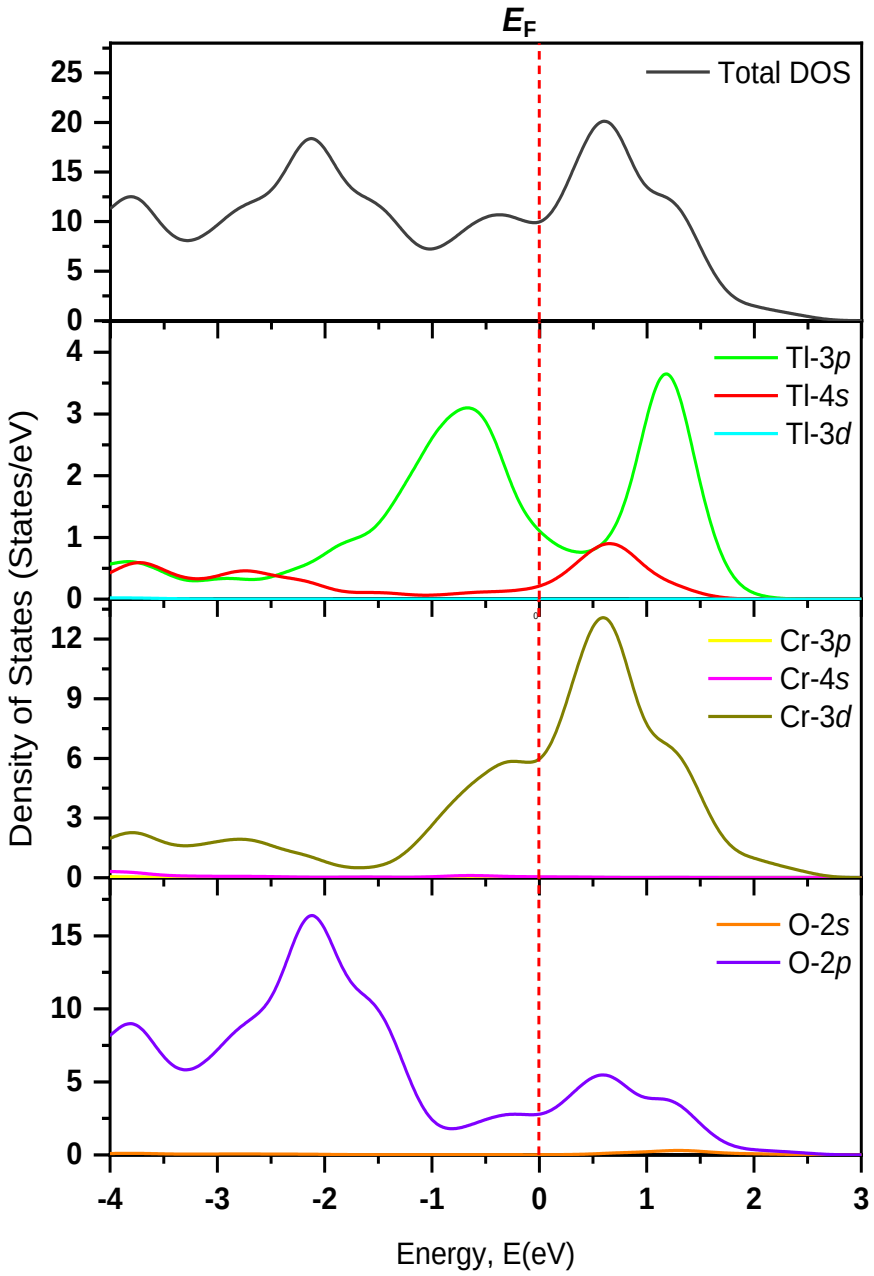

Figure 6.7 Total and partial DOS of $TlCrO_3$.

As a result, $TlCrO_3$ is less metallic. Major contribution near the Fermi level (E_F) derives from Cr-3*d* and Mn-3*d*. Here, Cr-3*d* seems to contribute more to the formation of the conduction band at ~0.6 eV. But Mn-3d contributes along the Fermi level making $TlMnO_3$ more metallic. $TlMnO_3$ shows a minor contribution along with E_F from the O-2*p* orbital. The orbitals also seem to have significant overlaps in energy, which point toward hybridization and inclination to the creation of covalent bonding. The values of

DOS are finite, which indicates $TlBO_3$(B = Cr, Mn) to be metallic. Moreover, the O-2*p* contributes to the creation of the valence band at ~ -2.1eV (for $TlCrO_3$) and ~ -2.2 (for $TlMnO_3$) states below the Fermi level (E_F). Hence, both perovskite materials are metallic. Two TDOS peaks for $TlMnO_3$ are found with close values at ~ -2.1eV and 0.7eV. $TlMnO_3$ has the largest TDOS peak at E_F again confirming it to have more metallic characteristics.

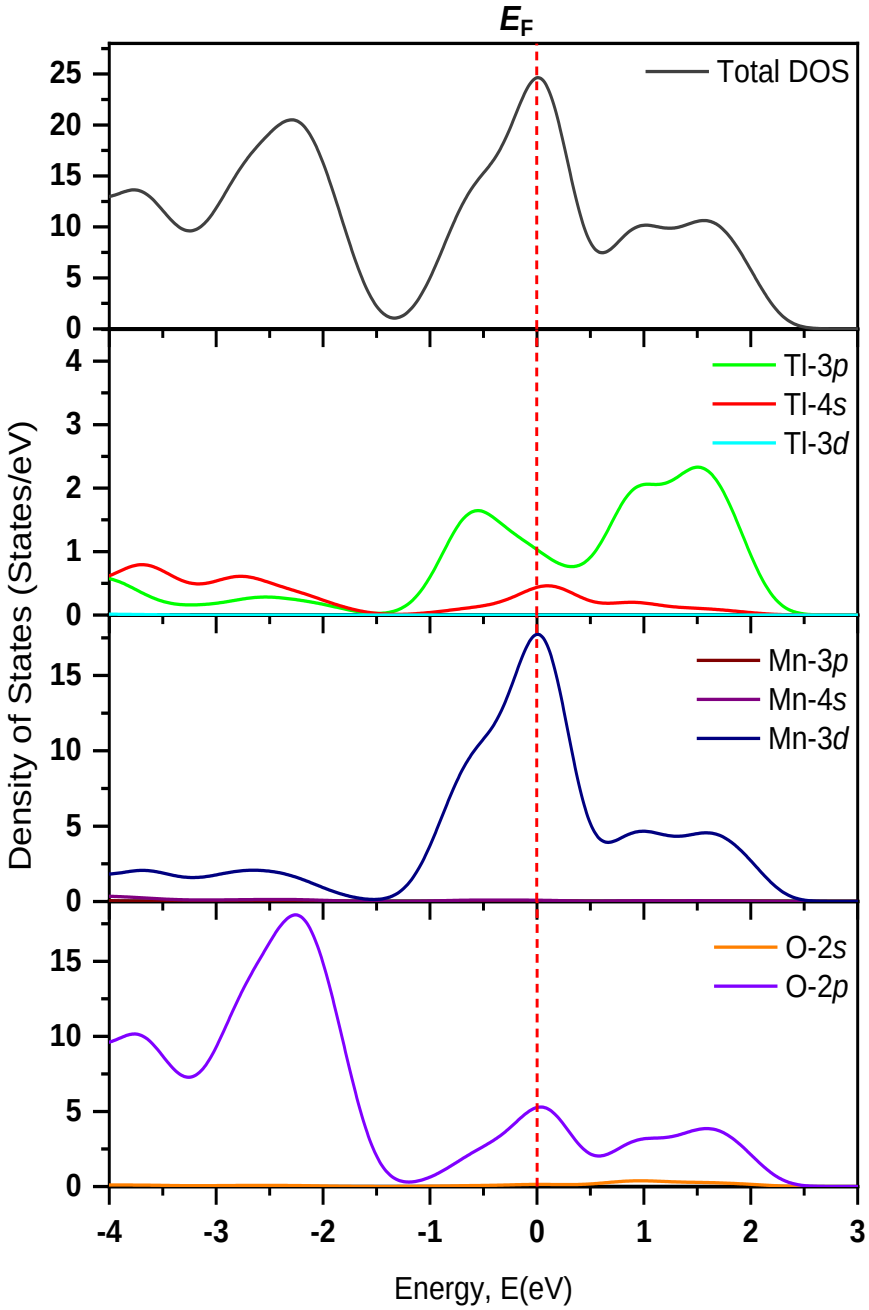

Figure 6.8 Total and partial DOS of $TlMnO_3$.

6.7. Optical properties

These properties are important for describing the response of solids to an occurrence of an electromagnetic wave and for exploring the potentiality of photovoltaic and optoelectronic devices. On that criterion, the performances of the materials to the infrared, visible, and ultraviolet spectra are particularly noteworthy. Various optical energy-dependent (frequency) parameters, which are the absorption co-efficient $\alpha(\omega)$, conductivity $\sigma(\omega)$, reflectivity $R(\omega)$, the real part of dielectric function $\varepsilon(\omega)$, loss function $L(\omega)$, and the refractive index $n(\omega)$ are calculated for photon energies up to 50 eV with electric field polarization vectors along [100] direction to analyse $TlBO_3$(B = Cr, Mn) as **Figure 6.9** depicted. The absorption spectrum is displayed in **Figure 6.9(a),** which shows expansion at inferior energies from ~0 to 15 eV due to transitions between close-lying energy levels including the band. However, $TlCrO_3$ shows a sharp peak at ~46eV in the higher energy band can be described as rapid transitions that occurred amongst the well-detached valence and conduction bands.

The peaks associated with the inter-band transitions are existing in the optical conductivity spectrum, which is presented in **Figure 6.9(b)**. A sharp edge can be seen for $TlMnO_3$ near UV region ~2eV and expansion can be seen for $TlCrO_3$ near ~4eV along with a sharp edge near ~46eV. In all-optical parameters near ~46eV is significant as it signifies a transition from metallic to dielectric in the character of solid. The reflectivity is presented in **Figure 6.9(c)**. The zero-frequency reflectivity (R (0)) is ~0.47 and ~0.71 for $TlCrO_3$ and $TlMnO_3$ respectively. A minor peak in the high-energy region is produced for $TlCrO_3$ due to inter-band carriers.

We considered the optical properties in the inter-band region. $\varepsilon(\omega)$ is generally measured by the inter-band along with inter-band optical transitions. For this investigation, we overlooked the indirect intra-band transition as this comprises phonon with an inadequate scattering cross-section compared to that of direct transition, as a result, phonon scattering is not required to recollect momentum. The ε (0) static dielectric constant is a significant optical parameter that is related to the semiconductor optical band gap and sometimes displays an opposite relationship with the values of the bandgap. **Figure 6.9(e)** represents the energy loss function, which means the loss of a fast-moving electron fleeting through the solid. The maximum energy loss in $TlCrO_3$ and $TlMnO_3$ occurs at ~9eV and ~12eV correspondingly. The energy-related to the peak is called plasma peak and the related frequency is named plasma frequency. Moreover, if more energy compared to plasma frequency was generated, the investigated materials would develop

transparency. Optical property, the refractive index holds a significant role from the standpoint of applications like solar cells, photonic crystals, and waveguides. The calculated values of the zero-frequency refractive index are ~9 and ~10 for the solids $TlCrO_3$ and $TlMnO_3$ respectively, as shown in **Figure 6.9(f)**. As the frequency is increased more than 10eV, the values of refractive index decrease for both materials, and slight non-linear nature can also be seen.

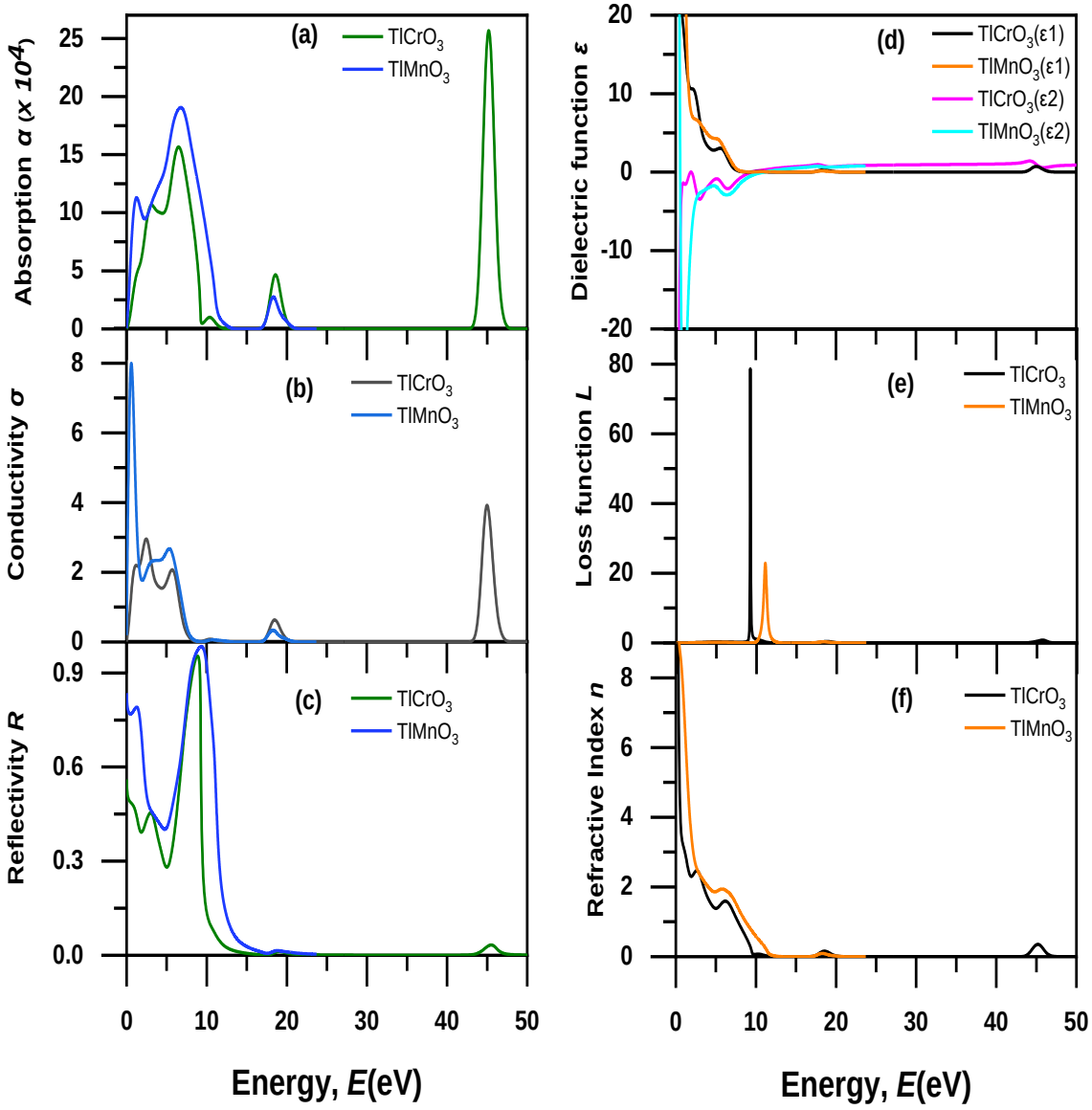

Figure 6.9 Energy-dependent (a) Absorption $\alpha(\omega)$, (b) Conductivity $\sigma(\omega)$, (c) Reflectivity $R(\omega)$, (d) Dielectric function $\varepsilon(\omega)$, (e) Loss function $L(\omega)$, and (f) Refractive index $n(\omega)$ of $TlBO_3$(B= Cr, Mn).

6.8. Thermodynamic properties

The thermodynamic properties of $TlBO_3$(B = Cr, Mn) are significant to find different demeanours of the solids under different pressure and temperature. Different variety of

thermodynamic properties can be measured such as Debye temperature (θ_D), melting temperature (T_m), and minimum thermal conductivity (K_{min}) using other properties like density (ρ), longitudinal, transverse, and average sound velocities ($\boldsymbol{v_l}$, $\boldsymbol{v_t}$, and v_m). The Debye temperature (θ_D) is evaluated as [139],

$$\theta_D = \frac{h}{k_B}\left[\frac{3m}{4\pi}\left(\frac{N_A\rho}{M}\right)\right]^{\frac{1}{3}} v_m. \tag{6.27}$$

Where h, k_B, V, v_m and n is Planck's constant, Boltzmann constant, unit cell volume, average sound velocity, and the number of atoms in the unite cell correspondingly. Here, v_m can be evaluated by the equation,

$$v_m = \left[\frac{1}{3}\left(\frac{2}{{v_t}^3} + \frac{1}{{v_l}^3}\right)\right]^{-\frac{1}{3}} \tag{6.28}$$

Where v_l is the transverse velocity and v_t is the longitudinal sound velocity of the solids. v_l and v_t are evaluated by the formula,

$$v_l = \left(\frac{B+\frac{4}{3}G}{\rho}\right) \tag{6.29}$$

$$v_t = \left[\frac{G}{\rho}\right]^{1/2} \tag{6.30}$$

The melting temperature (T_m) is also determined to explore the possible application of the materials at high temperatures. The following equation is used to determine (T_m) [140],

$$T_m = 354 + \frac{4.5(2C_{11}+C_{33})}{3} \tag{6.31}$$

Thermal conductivity, an important parameter to investigate the heat conduction of both $TlCrO_3$ and $TlMnO_3$ is determined. The minimum thermal conductivity (K_{min}) of solid material is associated with temperature and, will decrease to a certain value with a steady rise in temperature [141]. Minimum thermal conductivity (K_{min}) is calculated by Clarke formula [142].

$$K_{min} = k_B v_m \left(\frac{M}{\rho N_A n}\right)^{-2/3} \tag{6.32}$$

Where *M*, n, and N_A signify the molecular mass, atoms per molecule, and Avogadro's number correspondingly. The calculated thermal properties $\theta_D, T_m, K_{min}, v_m, v_t$ and v_l are presented in **Table 6.7**. The value of θ_D and K_{min} of both $TlCrO_3$ and $TlMnO_3$ reveals the possible application as a thermal barrier coating (TBC) for both solids [143]. The values of θ_D and K_{min} for the title compounds are much lower than the commercialized thermal barrier coating (TBC) compound, $Y_4Al_{12}O_9$ (K_{min} =1.13 W/mK; θ_D = 564 K) [143], [144].

Table 6.7 The calculated density (ρ), longitudinal, transverse, and average sound velocities $(v_l, v_t, and\ v_m)$, Debye temperature (θ_D), melting temperature (T_m), and minimum thermal conductivity (K_{min}) of $TlBO_3$(B = Cr, Mn) compound.

Compounds	**Crystal systems**	$\boldsymbol{\rho}$ **(g/cm^3)**	$\boldsymbol{v_l}$ **(km/s)**	$\boldsymbol{v_t}$ **(km/s)**	$\boldsymbol{v_m}$ **(km/s)**	$\boldsymbol{\theta_D}$ **(K)**	$\boldsymbol{T_m}$ **(K)**	$\boldsymbol{K_{min}}$ **(Wm^{-1}K^{-1})**
$TlCrO_3$	Orthorhombic	8.898	4.319	2.772	3.045	403.5	1697.53	0.83
$TlMnO_3$	Triclinic	8.982	3.898	2.514	2.760	365.7	1544.35	0.75

CHAPTER-7

CONCLUSIONS

The physical properties like structural, mechanical, elastic anisotropic, Vickers hardness, electronic, optical, and thermodynamic properties of $TlBO_3$(B = Cr, Mn) structure type perovskites are investigated for the first time in ab initio based DFT calculations. Good agreement is created between the values evaluated and considered elastic constants. Born criteria for both materials are fulfilled signifying that both solids are mechanically stable. Both materials are ductile as defined by all the elastic moduli like Cauchy pressure, Poisson's ratio, and Pugh's ratio. All the different methods employed for the anisotropy of $TlBO_3$(B = Cr, Mn) obtained the same results. The hardness calculations reveal both solids are flexible, soft, and suitable for making a thin film. The Vickers hardness value is also very to MAX phase materials. The investigation of optical properties of both $TlCrO_3$ and $TlMnO_3$ reveals various possible uses such as waveguides, ultra-large integration of integrated circuits, microelectronics, the reduction of solar heating, and optical fibre production. As the solids consist of lower values of θ_D and K_{min}, which implies they can be used as thermal barrier coating (TBC) material.

Future work:

We hope this investigation will help a researcher to use these materials for different applications according to their physical properties and also inspire scientists both experimentally and theoretically to discover this material in more depth both theoretically and experimentally in forthcoming.

REFERENCES

[1] H.-R. Wenk and A. G. Bulakh, *Minerals: their constitution and origin*. Cambridge ; New York: Cambridge University Press, 2004.

[2] N. Orlovskaya and N. Browning, *Mixed ionic electronic conducting perovskites for advanced energy systems*, vol. 173. Springer Science & Business Media, 2004.

[3] M. W. Lufaso and P. M. Woodward, "Jahn–Teller distortions, cation ordering and octahedral tilting in perovskites," *Acta Crystallogr B Struct Sci*, vol. 60, no. 1, pp. 10–20, Feb. 2004, doi: 10.1107/S0108768103026661.

[4] M. Johnsson and P. Lemmens, "Crystallography and Chemistry of Perovskites," in *Handbook of Magnetism and Advanced Magnetic Materials*, H. Kronmüller and S. Parkin, Eds. Chichester, UK: John Wiley & Sons, Ltd, 2007, p. hmm411. doi: 10.1002/9780470022184.hmm411.

[5] M. Becker, T. Klüner, and M. Wark, "Formation of hybrid ABX $_3$ perovskite compounds for solar cell application: first-principles calculations of effective ionic radii and determination of tolerance factors," *Dalton Trans.*, vol. 46, no. 11, pp. 3500–3509, 2017, doi: 10.1039/C6DT04796C.

[6] J. B. MacCHESNEY, J. J. Jetzt, J. F. Potter, H. J. Williams, and R. C. Sherwood, "Electrical and Magnetic Properties of the System SrFeO $_3$ -BiFeO $_3$," *Journal of the American Ceramic Society*, vol. 49, no. 12, pp. 644–647, Dec. 1966, doi: 10.1111/j.1151-2916.1966.tb13191.x.

[7] M. E. Lines, A. M. Glass, and G. Burns, "*Principles and Applications of Ferroelectrics and Related Materials*," *Physics Today*, vol. 31, no. 9, pp. 56–58, Sep. 1978, doi: 10.1063/1.2995188.

[8] G. Banach and W. M. Temmerman, "Delocalization and charge disproportionation in La (1 − x) Sr x MnO 3," *Phys. Rev. B*, vol. 69, no. 5, p. 054427, Feb. 2004, doi: 10.1103/PhysRevB.69.054427.

[9] S. Mathi Jaya, R. Jagadish, R. S. Rao, and R. Asokamani, "Electronic structure and magnetism of SrFeO 3 and SrCoO 3," *Phys. Rev. B*, vol. 43, no. 16, pp. 13274–13279, Jun. 1991, doi: 10.1103/PhysRevB.43.13274.

[10] L. F. Mattheiss, "Electronic Structure of the 3 d Transition-Metal Monoxides. I. Energy-Band Results," *Phys. Rev. B*, vol. 5, no. 2, pp. 290–306, Jan. 1972, doi: 10.1103/PhysRevB.5.290.

[11] N. F. Quackenbush *et al.*, "Nature of the Metal Insulator Transition in Ultrathin Epitaxial Vanadium Dioxide," *Nano Lett.*, vol. 13, no. 10, pp. 4857–4861, Oct. 2013, doi: 10.1021/nl402716d.

[12] E. Dagotto, "Complexity in Strongly Correlated Electronic Systems," *Science*, vol. 309, no. 5732, pp. 257–262, Jul. 2005, doi: 10.1126/science.1107559.

[13] A. V. Boris *et al.*, "Dimensionality Control of Electronic Phase Transitions in Nickel-Oxide Superlattices," *Science*, vol. 332, no. 6032, pp. 937–940, May 2011, doi: 10.1126/science.1202647.

[14] T.-H. Kim *et al.*, "Imaging and manipulation of the competing electronic phases near the Mott metal-insulator transition," *Proc. Natl. Acad. Sci. U.S.A.*, vol. 107, no. 12, pp. 5272–5275, Mar. 2010, doi: 10.1073/pnas.1000655107.

[15] C. Giannetti, M. Capone, D. Fausti, M. Fabrizio, F. Parmigiani, and D. Mihailovic, "Ultrafast optical spectroscopy of strongly correlated materials and high-temperature superconductors: a non-equilibrium approach," *Advances in Physics*, vol. 65, no. 2, pp. 58–238, Mar. 2016, doi: 10.1080/00018732.2016.1194044.

[16] M. Imada, A. Fujimori, and Y. Tokura, "Metal-insulator transitions," *Rev. Mod. Phys.*, vol. 70, no. 4, pp. 1039–1263, Oct. 1998, doi: 10.1103/RevModPhys.70.1039.

[17] J. Zaanen, G. A. Sawatzky, and J. W. Allen, “Band gaps and electronic structure of transition-metal compounds,” *Phys. Rev. Lett.*, vol. 55, no. 4, pp. 418–421, Jul. 1985, doi: 10.1103/PhysRevLett.55.418.

[18] K. Held, G. Keller, V. Eyert, D. Vollhardt, and V. I. Anisimov, “Mott-Hubbard Metal-Insulator Transition in Paramagnetic V 2 O 3 : An L D A + D M F T (QMC) Study,” *Phys. Rev. Lett.*, vol. 86, no. 23, pp. 5345–5348, Jun. 2001, doi: 10.1103/PhysRevLett.86.5345.

[19] Z. Shen and D. Dessau, “Physica Reports 253, 1 (1995); M Kozielski, I Pollini and G Spinolo,” *J. Phys C: Solid State Phys*, vol. 5, p. 1253, 1972.

[20] S. Nakamura, K. Nanba, and S. Iida, “Possible giant magnetoresistance effect in La1 − xAxMnO3 (A: Li, Na),” *Journal of Magnetism and Magnetic Materials*, vol. 177–181, pp. 884–885, Jan. 1998, doi: 10.1016/S0304-8853(97)00443-5.

[21] B. C. H. Steele and A. Heinzel, “Materials for fuel-cell technologies,” in *Materials for Sustainable Energy*, Co-Published with Macmillan Publishers Ltd, UK, 2010, pp. 224–231. doi: 10.1142/9789814317665_0031.

[22] A. J. Jacobson, “Materials for Solid Oxide Fuel Cells,” *Chem. Mater.*, vol. 22, no. 3, pp. 660–674, Feb. 2010, doi: 10.1021/cm902640j.

[23] T. Wolfram and S. Ellialtioglu, *Electronic and optical properties of D-band perovskites*. Cambridge, UK; New York: Cambridge University Press, 2006. Accessed: Apr. 28, 2022. [Online]. Available: https://doi.org/10.1017/CBO9780511541292

[24] Z. Feng, H. Hu, S. Cui, and C. Bai, “First-principles study of optical properties of SrZrO3 in cubic phase,” *Solid State Communications*, vol. 148, no. 9–10, pp. 472–475, Dec. 2008, doi: 10.1016/j.ssc.2008.08.030.

[25] S.-J. Kim, G. Demazeau, J. A. Alonso, and J.-H. Choy, “High pressure synthesis and crystal structure of a new Ni(III) perovskite: TlNiO3,” *J. Mater. Chem.*, vol. 11, no. 2, pp. 487–492, 2001, doi: 10.1039/b007043m.

[26] Z. Ali, I. Ahmad, I. Khan, and B. Amin, “Electronic structure of cubic perovskite SnTaO3,” *Intermetallics*, vol. 31, pp. 287–291, Dec. 2012, doi: 10.1016/j.intermet.2012.08.001.

[27] S. Takeno, R. Ohara, K. Sano, and T. Kawakubo, “Novel compositional accommodation mechanism in SrNbO3 epitaxial thin films revealed by analytical electron microscopy,” *Surf. Interface Anal.*, vol. 35, no. 1, pp. 29–35, Jan. 2003, doi: 10.1002/sia.1488.

[28] M. Yoshino, “Local electronic structures around hydrogen and acceptor ions in perovskite-type oxide, SrZrO3,” *Solid State Ionics*, vol. 127, no. 1–2, pp. 109–123, Jan. 2000, doi: 10.1016/S0167-2738(99)00274-X.

[29] Z. Fang *et al.*, “The Anomalous Hall Effect and Magnetic Monopoles in Momentum Space,” *Science*, vol. 302, no. 5642, pp. 92–95, Oct. 2003, doi: 10.1126/science.1089408.

[30] J. F. Scott, “Applications of Modern Ferroelectrics,” *Science*, vol. 315, no. 5814, pp. 954–959, Feb. 2007, doi: 10.1126/science.1129564.

[31] E. Cross, “Lead-free at last,” *Nature*, vol. 432, no. 7013, pp. 24–25, Nov. 2004, doi: 10.1038/nature03142.

[32] T. Schneider, D. Leduc, J. Cardin, C. Lupi, N. Barreau, and H. Gundel, “Optical properties of PZT thin films deposited on a ZnO buffer layer,” *Optical Materials*, vol. 29, no. 12, pp. 1871–1877, Aug. 2007, doi: 10.1016/j.optmat.2006.10.015.

[33] R. Watton, “Ferroelectric materials and devices in infrared detection and imaging,” *Ferroelectrics*, vol. 91, no. 1, pp. 87–108, Mar. 1989, doi: 10.1080/00150198908015731.

[34] R. D. Shannon, “Synthesis of some new perovskites containing indium and thallium,” *Inorg. Chem.*, vol. 6, no. 8, pp. 1474–1478, Aug. 1967, doi: 10.1021/ic50054a009.
[35] A. A. Belik, Y. Matsushita, M. Tanaka, and E. Takayama-Muromachi, “Crystal Structures and Properties of Perovskites $ScCrO_3$ and $InCrO_3$ with Small Ions at the A Site,” *Chem. Mater.*, vol. 24, no. 11, pp. 2197–2203, Jun. 2012, doi: 10.1021/cm3009144.
[36] W. Yi *et al.*, “High-pressure synthesis, crystal structure and magnetic properties of $TlCrO_3$ perovskite,” *Dalton Trans.*, vol. 44, no. 23, pp. 10785–10794, 2015, doi: 10.1039/C4DT03823A.
[37] S. Niitaka, “Crystal structure and dielectric and magnetic properties of BiCrO3 as a ferroelectromagnet,” *Solid State Ionics*, vol. 172, no. 1–4, pp. 557–559, Aug. 2004, doi: 10.1016/j.ssi.2004.01.060.
[38] C. Darie *et al.*, “Magnetic and crystal structures of BiCrO3,” *Solid State Sciences*, vol. 12, no. 5, pp. 660–664, May 2010, doi: 10.1016/j.solidstatesciences.2008.12.004.
[39] A. A. Belik, N. Tsujii, H. Suzuki, and E. Takayama-Muromachi, “Magnetic Properties of Bulk $BiCrO_3$ Studied with dc and ac Magnetization and Specific Heat,” *Inorg. Chem.*, vol. 46, no. 21, pp. 8746–8751, Oct. 2007, doi: 10.1021/ic701099f.
[40] A. V. Sobolev, A. V. Bokov, W. Yi, A. A. Belik, I. A. Presniakov, and I. S. Glazkova, “Electric Hyperfine Interactions of 57Fe Impurity Atoms in ACrO3 Perovskite-Type Chromites (A = Sc, In, Tl, Bi),” *J. Exp. Theor. Phys.*, vol. 129, no. 5, pp. 896–902, Nov. 2019, doi: 10.1134/S1063776119090127.
[41] K. Sardar, M. R. Lees, R. J. Kashtiban, J. Sloan, and R. I. Walton, “Direct Hydrothermal Synthesis and Physical Properties of Rare-Earth and Yttrium Orthochromite Perovskites,” *Chem. Mater.*, vol. 23, no. 1, pp. 48–56, Jan. 2011, doi: 10.1021/cm102925z.
[42] T. Kimura, T. Goto, H. Shintani, K. Ishizaka, T. Arima, and Y. Tokura, “Magnetic control of ferroelectric polarization,” *Nature*, vol. 426, no. 6962, pp. 55–58, Nov. 2003, doi: 10.1038/nature02018.
[43] M. Fiebig, Th. Lottermoser, D. Fröhlich, A. V. Goltsev, and R. V. Pisarev, “Observation of coupled magnetic and electric domains,” *Nature*, vol. 419, no. 6909, pp. 818–820, Oct. 2002, doi: 10.1038/nature01077.
[44] Y. Kumagai, A. A. Belik, M. Lilienblum, N. Leo, M. Fiebig, and N. A. Spaldin, “Observation of persistent centrosymmetricity in the hexagonal manganite family,” *Phys. Rev. B*, vol. 85, no. 17, p. 174422, May 2012, doi: 10.1103/PhysRevB.85.174422.
[45] S. Lee *et al.*, “Giant magneto-elastic coupling in multiferroic hexagonal manganites,” *Nature*, vol. 451, no. 7180, pp. 805–808, Feb. 2008, doi: 10.1038/nature06507.
[46] M. Tachibana, T. Shimoyama, H. Kawaji, T. Atake, and E. Takayama-Muromachi, “Jahn-Teller distortion and magnetic transitions in perovskite R Mn O 3 (R = Ho , Er, Tm, Yb, and Lu),” *Phys. Rev. B*, vol. 75, no. 14, p. 144425, Apr. 2007, doi: 10.1103/PhysRevB.75.144425.
[47] V. Yu Pomjakushin *et al.*, “Evidence for large electric polarization from collinear magnetism in $TmMnO_3$,” *New J. Phys.*, vol. 11, no. 4, p. 043019, Apr. 2009, doi: 10.1088/1367-2630/11/4/043019.
[48] B. Rajeswaran, D. I. Khomskii, A. K. Zvezdin, C. N. R. Rao, and A. Sundaresan, “Field-induced polar order at the Néel temperature of chromium in rare-earth

orthochromites: Interplay of rare-earth and Cr magnetism," *Phys. Rev. B*, vol. 86, no. 21, p. 214409, Dec. 2012, doi: 10.1103/PhysRevB.86.214409.
[49] C. R. Serrao, A. K. Kundu, S. B. Krupanidhi, U. V. Waghmare, and C. N. R. Rao, "Biferroic Y Cr O 3," *Phys. Rev. B*, vol. 72, no. 22, p. 220101, Dec. 2005, doi: 10.1103/PhysRevB.72.220101.
[50] J.-S. Zhou *et al.*, "Intrinsic structural distortion and superexchange interaction in the orthorhombic rare-earth perovskites R CrO 3," *Phys. Rev. B*, vol. 81, no. 21, p. 214115, Jun. 2010, doi: 10.1103/PhysRevB.81.214115.
[51] T. Goto, T. Kimura, G. Lawes, A. P. Ramirez, and Y. Tokura, "Ferroelectricity and Giant Magnetocapacitance in Perovskite Rare-Earth Manganites," *Phys. Rev. Lett.*, vol. 92, no. 25, p. 257201, Jun. 2004, doi: 10.1103/PhysRevLett.92.257201.
[52] Y. Tokunaga, S. Iguchi, T. Arima, and Y. Tokura, "Magnetic-Field-Induced Ferroelectric State in DyFeO 3," *Phys. Rev. Lett.*, vol. 101, no. 9, p. 097205, Aug. 2008, doi: 10.1103/PhysRevLett.101.097205.
[53] A. Paul, A. Mukherjee, I. Dasgupta, A. Paramekanti, and T. Saha-Dasgupta, "Hybridization-switching induced Mott transition in ABO$_3$ perovskites," *Phys. Rev. Lett.*, vol. 122, no. 1, p. 016404, Jan. 2019, doi: 10.1103/PhysRevLett.122.016404.
[54] W. Yi *et al.*, "Perovskite-Structure $TlMnO_3$: A New Manganite with New Properties," *Inorg. Chem.*, vol. 53, no. 18, pp. 9800–9808, Sep. 2014, doi: 10.1021/ic501380m.
[55] D. D. Khalyavin, P. Manuel, W. Yi, and A. A. Belik, "Spin and orbital ordering in TlMnO 3 : Neutron diffraction study," *Phys. Rev. B*, vol. 94, no. 13, p. 134412, Oct. 2016, doi: 10.1103/PhysRevB.94.134412.
[56] A. A. Belik, "Structural, magnetic, and dielectric properties of solid solutions between BiMnO3 and YMnO3," *Journal of Solid State Chemistry*, vol. 246, pp. 8–15, Feb. 2017, doi: 10.1016/j.jssc.2016.10.025.
[57] M. L. Keith and R. Roy, "Structural relations among double oxides of trivalent elements," *American Mineralogist*, vol. 39, no. 1–2, pp. 1–23, Feb. 1954.
[58] ROTH R. S., "Classification of Perovskite and Other ABO_3-Type Compounds," *Journal of Research of the National Bureau of Standards*, vol. 58, no. 2, pp. 75–88, 1957.
[59] Z. Ali, I. Ahmad, and A. H. Reshak, "GGA+U studies of the cubic perovskites BaMO3 (M=Pr, Th and U)," *Physica B: Condensed Matter*, vol. 410, pp. 217–221, Feb. 2013, doi: 10.1016/j.physb.2012.11.008.
[60] Z. Ali and I. Ahmad, "Band Profile Comparison of the Cubic Perovskites CaCoO3 and SrCoO3," *Journal of Elec Materi*, vol. 42, no. 3, pp. 438–444, Mar. 2013, doi: 10.1007/s11664-012-2377-y.
[61] L. Feng, Z. Liu, and Q. Liu, "Structural, elastic and mechanical properties of orthorhombic SrHfO3 under pressure from first-principles calculations," *Physica B: Condensed Matter*, vol. 407, no. 12, pp. 2009–2013, Jun. 2012, doi: 10.1016/j.physb.2012.01.130.
[62] Z. Hasan, Rasheduzzaman, and K. Monower Hossain, "Investigations on pressure dependent physical properties of cubic $AMoO_3$ (A = Ca, Sr) perovskites: A DFT calculation," *International Journal of Materials Research*, vol. 111, no. 12, pp. 1038–1046, Dec. 2020, doi: 10.3139/146.111969.
[63] M. Z. Hasan, M. Rasheduzzaman, and K. Monower Hossain, "Pressure-dependent physical properties of cubic $SrBO_3$ (B = Cr, Fe) perovskites investigated by density functional theory*," *Chinese Phys. B*, vol. 29, no. 12, p. 123101, Dec. 2020, doi: 10.1088/1674-1056/abab7f.

[64] Md. Z. Hasan, K. M. Hossain, S. K. Mitro, Md. Rasheduzzaman, J. K. Modak, and M. A. Rayhan, "Structural, mechanical, electronic, and anisotropic properties of niobium-doped strontium ferrite: first-principle calculations," *Appl. Phys. A*, vol. 127, no. 1, p. 36, Jan. 2021, doi: 10.1007/s00339-020-04219-5.

[65] E. F. Bertaut, A. Delapalme, F. Forrat, G. Roult, F. De Bergevin, and R. Pauthenet, "Magnetic Structure Work at the Nuclear Center of Grenoble," *Journal of Applied Physics*, vol. 33, no. 3, pp. 1123–1124, Mar. 1962, doi: 10.1063/1.1728627.

[66] N. Shamir, H. Shaked, and S. Shtrikman, "Magnetic structure of some rare-earth orthochromites," *Phys. Rev. B*, vol. 24, no. 11, pp. 6642–6651, Dec. 1981, doi: 10.1103/PhysRevB.24.6642.

[67] C. V. Colin, A. G. Pérez, P. Bordet, C. Goujon, and C. Darie, "Symmetry adapted analysis of the magnetic and structural phase diagram of Bi 1 − x Y x CrO 3," *Phys. Rev. B*, vol. 85, no. 22, p. 224103, Jun. 2012, doi: 10.1103/PhysRevB.85.224103.

[68] G. Demazeau, A. Marbeuf, M. Pouchard, and P. Hagenmuller, "Sur une série de composés oxygènes du nickel trivalent derivés de la perovskite," *Journal of Solid State Chemistry*, vol. 3, no. 4, pp. 582–589, Nov. 1971, doi: 10.1016/0022-4596(71)90105-8.

[69] S. J. Kim *et al.*, "The Ni(III) perovskites: synthesis under high oxygen pressures and physico-chemical properties," *Solid State Communications*, vol. 117, no. 2, pp. 113–115, Dec. 2000, doi: 10.1016/S0038-1098(00)00419-1.

[70] Y. Cao *et al.*, "Magnetization switching of rare earth orthochromite $CeCrO_3$," *Appl. Phys. Lett.*, vol. 104, no. 23, p. 232405, Jun. 2014, doi: 10.1063/1.4882642.

[71] M. Itoh, J. Hashimoto, S. Yamaguchi, and Y. Tokura, "Spin state and metal–insulator transition in LaCoO3 and RCoO3 (R=Nd, Sm and Eu)," *Physica B: Condensed Matter*, vol. 281–282, pp. 510–511, Jun. 2000, doi: 10.1016/S0921-4526(99)01044-3.

[72] L. Ding *et al.*, "Unusual magnetic structure of the high-pressure synthesized perovskites A CrO 3 (A = Sc , In, Tl)," *Phys. Rev. B*, vol. 95, no. 5, p. 054432, Feb. 2017, doi: 10.1103/PhysRevB.95.054432.

[73] S. Clark and M. Segall, "CJ pickard, PJ Hasnip, MJ Probert, K. Refson, and MC Payne," *Z. Kristallogr*, vol. 220, p. 567, 2005.

[74] J. P. Perdew *et al.*, "Erratum: Restoring the Density-Gradient Expansion for Exchange in Solids and Surfaces [Phys. Rev. Lett. 100, 136406 (2008)]," *Phys. Rev. Lett.*, vol. 102, no. 3, p. 039902, Jan. 2009, doi: 10.1103/PhysRevLett.102.039902.

[75] P. Hohenberg and W. Kohn, "Inhomogeneous Electron Gas," *Phys. Rev.*, vol. 136, no. 3B, pp. B864–B871, Nov. 1964, doi: 10.1103/PhysRev.136.B864.

[76] M. D. Segall *et al.*, "First-principles simulation: ideas, illustrations and the CASTEP code," *J. Phys.: Condens. Matter*, vol. 14, no. 11, pp. 2717–2744, Mar. 2002, doi: 10.1088/0953-8984/14/11/301.

[77] H. J. Monkhorst and J. D. Pack, "Special points for Brillouin-zone integrations," *Phys. Rev. B*, vol. 13, no. 12, pp. 5188–5192, Jun. 1976, doi: 10.1103/PhysRevB.13.5188.

[78] B. G. Pfrommer, M. Côté, S. G. Louie, and M. L. Cohen, "Relaxation of Crystals with the Quasi-Newton Method," *Journal of Computational Physics*, vol. 131, no. 1, pp. 233–240, Feb. 1997, doi: 10.1006/jcph.1996.5612.

[79] C.-Z. Fan *et al.*, "Potential superhard osmium dinitride with fluorite and pyrite structure: First-principles calculations," *Phys. Rev. B*, vol. 74, no. 12, p. 125118, Sep. 2006, doi: 10.1103/PhysRevB.74.125118.

[80] R. Gaillac, P. Pullumbi, and F.-X. Coudert, “ELATE: An open-source online application for analysis and visualization of elastic tensors,” *J. Phys.: Condens. Matter*, vol. 28, no. 27, p. 275201, Jul. 2016, doi: 10.1088/0953-8984/28/27/275201.
[81] S. J. Clark *et al.*, “First principles methods using CASTEP,” *Zeitschrift für Kristallographie - Crystalline Materials*, vol. 220, no. 5–6, pp. 567–570, May 2005, doi: 10.1524/zkri.220.5.567.65075.
[82] “Atomic Orbital Theory,” in *The Vocabulary and Concepts of Organic Chemistry*, Hoboken, NJ, USA: John Wiley & Sons, Inc., 2005, pp. 1–24. doi: 10.1002/0471713740.ch1.
[83] J. Daintith, Ed., *A dictionary of chemistry*, 5th ed. Oxford ; New York: Oxford University Press, 2004.
[84] E. Schrödinger, “Quantisierung als Eigenwertproblem,” *Ann. Phys.*, vol. 384, no. 4, pp. 361–376, 1926, doi: 10.1002/andp.19263840404.
[85] J. E. Huheey, E. A. Keiter, R. L. Keiter, and O. K. Medhi, *Inorganic chemistry: principles of structure and reactivity*. 2013.
[86] “The quantum theory of the electron,” *Proc. R. Soc. Lond. A*, vol. 117, no. 778, pp. 610–624, Feb. 1928, doi: 10.1098/rspa.1928.0023.
[87] J. C. Slater, “A Simplification of the Hartree-Fock Method,” *Phys. Rev.*, vol. 81, no. 3, pp. 385–390, Feb. 1951, doi: 10.1103/PhysRev.81.385.
[88] C. J. Cramer, *Essentials of computational chemistry: theories and models*, 2nd ed. Chichester, West Sussex, England ; Hoboken, NJ: Wiley, 2004.
[89] F. Jensen, *Introduction to computational chemistry*, 2nd ed. Chichester, England ; Hoboken, NJ: John Wiley & Sons, 2007.
[90] V. Saunders *et al.*, “CRYSTAL98 user’s manual,” *University of Torino, Torino*, vol. 230, 1998.
[91] D. R. Hartree, “The Wave Mechanics of an Atom with a Non-Coulomb Central Field. Part I. Theory and Methods,” *Math. Proc. Camb. Phil. Soc.*, vol. 24, no. 1, pp. 89–110, Jan. 1928, doi: 10.1017/S0305004100011919.
[92] C. C. J. Roothaan, “New Developments in Molecular Orbital Theory,” *Rev. Mod. Phys.*, vol. 23, no. 2, pp. 69–89, Apr. 1951, doi: 10.1103/RevModPhys.23.69.
[93] P. Hohenberg and W. Kohn, “Density functional theory (DFT),” *Phys. Rev*, vol. 136, p. B864, 1964.
[94] W. Kohn and L. J. Sham, “Self-Consistent Equations Including Exchange and Correlation Effects,” *Phys. Rev.*, vol. 140, no. 4A, pp. A1133–A1138, Nov. 1965, doi: 10.1103/PhysRev.140.A1133.
[95] G. L. Zhao, D. Bagayoko, and T. D. Williams, “Local-density-approximation prediction of electronic properties of GaN, Si, C, and RuO 2,” *Phys. Rev. B*, vol. 60, no. 3, pp. 1563–1572, Jul. 1999, doi: 10.1103/PhysRevB.60.1563.
[96] F. W. Kutzler and G. S. Painter, “First-row diatomics: Calculation of the geometry and energetics using self-consistent gradient-functional approximations,” *Phys. Rev. B*, vol. 45, no. 7, pp. 3236–3244, Feb. 1992, doi: 10.1103/PhysRevB.45.3236.
[97] D. R. Hamann, M. Schlüter, and C. Chiang, “Norm-Conserving Pseudopotentials,” *Phys. Rev. Lett.*, vol. 43, no. 20, pp. 1494–1497, Nov. 1979, doi: 10.1103/PhysRevLett.43.1494.
[98] R. D. King-Smith, M. C. Payne, and J. S. Lin, “Real-space implementation of nonlocal pseudopotentials for first-principles total-energy calculations,” *Phys. Rev. B*, vol. 44, no. 23, pp. 13063–13066, Dec. 1991, doi: 10.1103/PhysRevB.44.13063.
[99] C. Pisani, *Quantum-mechanical ab-initio calculation of the properties of crystalline materials*, vol. 67. Springer Science & Business Media, 2012.

[100] R. Dovesi, “On the role of symmetry in the ab initio hartree-fock linear-combination-of-atomic-orbitals treatment of periodic systems,” *Int. J. Quantum Chem.*, vol. 29, no. 6, pp. 1755–1774, Jun. 1986, doi: 10.1002/qua.560290608.
[101] M. C. Payne, M. P. Teter, D. C. Allan, T. A. Arias, and J. D. Joannopoulos, “Iterative minimization techniques for *ab initio* total-energy calculations: molecular dynamics and conjugate gradients,” *Rev. Mod. Phys.*, vol. 64, no. 4, pp. 1045–1097, Oct. 1992, doi: 10.1103/RevModPhys.64.1045.
[102] L. Kleinman and D. M. Bylander, “Efficacious Form for Model Pseudopotentials,” *Phys. Rev. Lett.*, vol. 48, no. 20, pp. 1425–1428, May 1982, doi: 10.1103/PhysRevLett.48.1425.
[103] D. Vanderbilt, “Soft self-consistent pseudopotentials in a generalized eigenvalue formalism,” *Phys. Rev. B*, vol. 41, no. 11, pp. 7892–7895, Apr. 1990, doi: 10.1103/PhysRevB.41.7892.
[104] G. Kresse and J. Furthmüller, “Efficient iterative schemes for *ab initio* total-energy calculations using a plane-wave basis set,” *Phys. Rev. B*, vol. 54, no. 16, pp. 11169–11186, Oct. 1996, doi: 10.1103/PhysRevB.54.11169.
[105] D. Alfè, “Ab initio molecular dynamics, a simple algorithm for charge extrapolation,” *Computer Physics Communications*, vol. 118, no. 1, pp. 31–33, Apr. 1999, doi: 10.1016/S0010-4655(98)00195-7.
[106] N. Marzari, D. Vanderbilt, and M. C. Payne, “Ensemble Density-Functional Theory for *Ab Initio* Molecular Dynamics of Metals and Finite-Temperature Insulators,” *Phys. Rev. Lett.*, vol. 79, no. 7, pp. 1337–1340, Aug. 1997, doi: 10.1103/PhysRevLett.79.1337.
[107] S.-Y. Yoon, J.-K. Kim, and K. H. Kim, “A comparative study on tribological behavior of TiN and TiAlN coatings prepared by arc ion plating technique,” *Surface and Coatings Technology*, vol. 161, no. 2–3, pp. 237–242, Dec. 2002, doi: 10.1016/S0257-8972(02)00474-7.
[108] C. A. Coulson, “Physical Properties of Crystals. By J. F. Nye . Pp. xv, 322, 50s. 1957. (Oxford: Clarendon Press),” *Math. Gaz.*, vol. 42, no. 342, pp. 329–330, Dec. 1958, doi: 10.2307/3610487.
[109] G. Shi *et al.*, “Finding the Next Deep-Ultraviolet Nonlinear Optical Material: $NH_4B_4O_6F$,” *J. Am. Chem. Soc.*, vol. 139, no. 31, pp. 10645–10648, Aug. 2017, doi: 10.1021/jacs.7b05943.
[110] C. Ambrosch-Draxl and R. Abt, “The calculation of optical properties within WIEN97,” *ICTP Lecture Notes*, 1998.
[111] 嶽山正二郎, “PY Yu and M. Cardona, Fundamentals of Semiconductors; Physics and Materials Properties, Springer-Verlag, Berlin and Heidelberg, 1996, 617p., 15.4× 23.5 cm, 7,481 円 [大学院向],” 日本物理学会誌, vol. 53, no. 5, pp. 359–360, 1998.
[112] M. Fox and G. F. Bertsch, “*Optical Properties of Solids*,” *American Journal of Physics*, vol. 70, no. 12, pp. 1269–1270, Dec. 2002, doi: 10.1119/1.1691372.
[113] A. Delin *et al.*, “Optical properties of the group-IV *B* refractory metal compounds,” *Phys. Rev. B*, vol. 54, no. 3, pp. 1673–1681, Jul. 1996, doi: 10.1103/PhysRevB.54.1673.
[114] R. Majumder and M. M. Hossain, “First-principles study of structural, electronic, elastic, thermodynamic and optical properties of topological superconductor LuPtBi,” *Computational Condensed Matter*, vol. 21, p. e00402, Dec. 2019, doi: 10.1016/j.cocom.2019.e00402.
[115] C. Truesdell, “FD Murnaghan, Finite deformation of an elastic solid,” *Bulletin of the American Mathematical Society*, vol. 58, no. 5, pp. 577–579, 1952.

[116] J. Wang, S. Yip, S. R. Phillpot, and D. Wolf, “Crystal instabilities at finite strain,” *Phys. Rev. Lett.*, vol. 71, no. 25, pp. 4182–4185, Dec. 1993, doi: 10.1103/PhysRevLett.71.4182.
[117] D. C. Wallace, “Thermodynamics of Crystals John Wiley & Sons,” *New York*, 1972.
[118] H. Qin *et al.*, “First-principles study of structural, elastic, and electronic properties of triclinic TATB under different pressures,” *Physica B: Condensed Matter*, vol. 552, pp. 151–158, Jan. 2019, doi: 10.1016/j.physb.2018.10.003.
[119] D. H. Chung and W. R. Buessem, “The Elastic Anisotropy of Crystals,” *Journal of Applied Physics*, vol. 38, no. 5, pp. 2010–2012, Apr. 1967, doi: 10.1063/1.1709819.
[120] X. Gao, Y. Jiang, R. Zhou, and J. Feng, “Stability and elastic properties of Y–C binary compounds investigated by first principles calculations,” *Journal of Alloys and Compounds*, vol. 587, pp. 819–826, Feb. 2014, doi: 10.1016/j.jallcom.2013.11.005.
[121] P. Ravindran, L. Fast, P. A. Korzhavyi, B. Johansson, J. Wills, and O. Eriksson, “Density functional theory for calculation of elastic properties of orthorhombic crystals: Application to TiSi2,” *Journal of Applied Physics*, vol. 84, no. 9, pp. 4891–4904, Nov. 1998, doi: 10.1063/1.368733.
[122] W. Voigt, “Lehrbuch der Kristallphysik: Teubner-Leipzig,” 1928.
[123] A. Reuss, “Berechnung der Fließgrenze von Mischkristallen auf Grund der Plastizitätsbedingung für Einkristalle .,” *Z. angew. Math. Mech.*, vol. 9, no. 1, pp. 49–58, 1929, doi: 10.1002/zamm.19290090104.
[124] R. Hill, “The Elastic Behaviour of a Crystalline Aggregate,” *Proc. Phys. Soc. A*, vol. 65, no. 5, pp. 349–354, May 1952, doi: 10.1088/0370-1298/65/5/307.
[125] J. Maibam, B. Indrajit Sharma, R. Bhattacharjee, R. K. Thapa, and R. K. Brojen Singh, “Electronic structure and elastic properties of scandium carbide and yttrium carbide: A first principles study,” *Physica B: Condensed Matter*, vol. 406, no. 21, pp. 4041–4045, Nov. 2011, doi: 10.1016/j.physb.2011.07.036.
[126] S. F. Pugh, “XCII. Relations between the elastic moduli and the plastic properties of polycrystalline pure metals,” *The London, Edinburgh, and Dublin Philosophical Magazine and Journal of Science*, vol. 45, no. 367, pp. 823–843, Aug. 1954, doi: 10.1080/14786440808520496.
[127] Md. L. Ali and Md. Z. Rahaman, “Investigation of different physical aspects such as structural, mechanical, optical properties and Debye temperature of Fe_2ScM (M=P and As) semiconductors: A DFT-based first principles study,” *Int. J. Mod. Phys. B*, vol. 32, no. 10, p. 1850121, Apr. 2018, doi: 10.1142/S0217979218501217.
[128] D. G. Pettifor, “Theoretical predictions of structure and related properties of intermetallics,” *Materials Science and Technology*, vol. 8, no. 4, pp. 345–349, Apr. 1992, doi: 10.1179/mst.1992.8.4.345.
[129] M. H. K. Rubel, K. M. Hossain, S. K. Mitro, M. M. Rahaman, M. A. Hadi, and A. K. M. A. Islam, “Comprehensive first-principles calculations on physical properties of ScV2Ga4 and ZrV2Ga4 in comparison with superconducting HfV2Ga4,” *Materials Today Communications*, vol. 24, p. 100935, Sep. 2020, doi: 10.1016/j.mtcomm.2020.100935.
[130] R. Majumder, S. K. Mitro, and B. Bairagi, “Influence of metalloid antimony on the physical properties of palladium-based half-Heusler compared to the metallic bismuth: A first-principle study,” *Journal of Alloys and Compounds*, vol. 836, p. 155395, Sep. 2020, doi: 10.1016/j.jallcom.2020.155395.

[131] C. M. Kube, “Elastic anisotropy of crystals,” *AIP Advances*, vol. 6, no. 9, p. 095209, Sep. 2016, doi: 10.1063/1.4962996.
[132] A. Gueddouh, B. Bentria, and I. K. Lefkaier, “First-principle investigations of structure, elastic and bond hardness of FexB (x=1, 2, 3) under pressure,” *Journal of Magnetism and Magnetic Materials*, vol. 406, pp. 192–199, May 2016, doi: 10.1016/j.jmmm.2016.01.013.
[133] H. Gou, L. Hou, J. Zhang, and F. Gao, “Pressure-induced incompressibility of ReC and effect of metallic bonding on its hardness,” *Appl. Phys. Lett.*, vol. 92, no. 24, p. 241901, Jun. 2008, doi: 10.1063/1.2938031.
[134] F. Gao, “Theoretical model of intrinsic hardness,” *Phys. Rev. B*, vol. 73, no. 13, p. 132104, Apr. 2006, doi: 10.1103/PhysRevB.73.132104.
[135] M. A. Ali, M. A. Hadi, M. M. Hossain, S. H. Naqib, and A. K. M. A. Islam, “Theoretical investigation of structural, elastic, and electronic properties of ternary boride MoAlB: Theoretical investigation of ternary boride MoAlB,” *Phys. Status Solidi B*, vol. 254, no. 7, p. 1700010, Jul. 2017, doi: 10.1002/pssb.201700010.
[136] A. Chowdhury, M. A. Ali, M. M. Hossain, M. M. Uddin, S. H. Naqib, and A. K. M. A. Islam, “Predicted MAX Phase Sc $_2$ InC: Dynamical Stability, Vibrational and Optical Properties,” *Phys. Status Solidi B*, vol. 255, no. 3, p. 1700235, Mar. 2018, doi: 10.1002/pssb.201700235.
[137] M. I. Kholil, M. S. Ali, and M. Aftabuzzaman, “Structural, elastic, electronic and vibrational properties of BaRh2P2 and SrIr2As2 superconductors: A DFT study,” *Journal of Alloys and Compounds*, vol. 740, pp. 754–765, Apr. 2018, doi: 10.1016/j.jallcom.2017.09.209.
[138] P. Barua, M. M. Hossain, M. A. Ali, M. M. Uddin, S. H. Naqib, and A. K. M. A. Islam, “Effects of transition metals on physical properties of M2BC (M = V, Nb, Mo and Ta): A DFT calculation,” *Journal of Alloys and Compounds*, vol. 770, pp. 523–534, Jan. 2019, doi: 10.1016/j.jallcom.2018.08.155.
[139] O. L. Anderson, “A simplified method for calculating the debye temperature from elastic constants,” *Journal of Physics and Chemistry of Solids*, vol. 24, no. 7, pp. 909–917, Jul. 1963, doi: 10.1016/0022-3697(63)90067-2.
[140] M. E. Fine, L. D. Brown, and H. L. Marcus, “Elastic constants versus melting temperature in metals,” *Scripta Metallurgica*, vol. 18, no. 9, pp. 951–956, Sep. 1984, doi: 10.1016/0036-9748(84)90267-9.
[141] Y. Shen, D. R. Clarke, and P. A. Fuierer, “Anisotropic thermal conductivity of the Aurivillus phase, bismuth titanate (Bi4Ti3O12): A natural nanostructured superlattice,” *Appl. Phys. Lett.*, vol. 93, no. 10, p. 102907, Sep. 2008, doi: 10.1063/1.2975163.
[142] D. R. Clarke, “Materials selection guidelines for low thermal conductivity thermal barrier coatings,” *Surface and Coatings Technology*, vol. 163–164, pp. 67–74, Jan. 2003, doi: 10.1016/S0257-8972(02)00593-5.
[143] M. H. K. Rubel *et al.*, “Density functional theory study of a new Bi-based (K1.00)(Ba1.00)3(Bi0.89Na0.11)4O12 double perovskite superconductor,” *Computational Materials Science*, vol. 138, pp. 160–165, Oct. 2017, doi: 10.1016/j.commatsci.2017.06.030.
[144] Y. Zhou, H. Xiang, X. Lu, Z. Feng, and Z. Li, “Theoretical prediction on mechanical and thermal properties of a promising thermal barrier material: Y4Al2O9,” *J Adv Ceram*, vol. 4, no. 2, pp. 83–93, Jun. 2015, doi: 10.1007/s40145-015-0140-6.